Decentralized Consensus Control of a Rigid-Body Spacecraft Formation with Communication Delay

Decentralized Consensus Control of a Rigid Body Spacecraft Formation with Communication Delay

Morad Nazari*and Eric A. Butcher,†

University of Arizona, Tucson, Arizona 85721

Tansel Yucelen‡,

Missouri University of Science and Technology, Rolla, Missouri 65409

and

Amit K. Sanyal§

Syracuse University, Syracuse, New York 13244

DOI: 10.2514/1.G001396

Abstract

The decentralized consensus control of a formation of rigid body spacecraft is studied in the framework of geometric mechanics while accounting for a constant communication time delay between spacecraft. The relative position and attitude (relative pose) are represented on the Lie group SE(3) while the communication topology is modeled as a digraph. The consensus problem is converted into a local stabilization problem of the error dynamics associated with the Lie algebra $\mathfrak{se}(3)$ in the form of linear time-invariant delay differential equations (DDEs) with a single discrete delay in the case of a circular orbit while it is in the form of linear time-periodic DDEs in the case of an elliptic orbit, in which the stability may be assessed using infinite-dimensional Floquet

*Postdoctoral Researcher, Department of Aerospace and Mechanical Engineering. Member AIAA.

†Associate Professor, Department of Aerospace and Mechanical Engineering. Member AIAA.

‡Assistant Professor, Department of Mechanical and Aerospace Engineering. Member AIAA.

§Associate Professor, Mechanical and Aerospace Engineering Department. Member AIAA.

theory. The proposed technique is applied to the consensus control of four spacecraft in the vicinity of a Molniya orbit.

1 Introduction

In the control of spacecraft formations including formation establishment and maintenance, several types of desired configurations and control strategies have been introduced [1]. Among different control techniques, the leader-follower approach has been widely used in formation control. However, since the leader does not usually receive explicit information from the follower, a small perturbation in the follower due to disturbances can cause failure in the formation [2]. On the other hand, the loss of a leader can result in mission malfunction while leaderless networks are more robust to such cases since the agents do not have to receive explicit information from a leader. In related papers, control strategies are designed based on the assumption that each agent tracks its adjacent agent's states [3] and hence the loss of one agent is likely to cause the controller to fail. However, leaderless consensus algorithms are capable of managing such cases since they do not rely on specific agents. Therefore, the necessity for considering leaderless consensus for geometric configuration establishment and maintenance between multiple spacecraft arises.

Several papers have considered the decentralized attitude control design where the spacecraft in formation achieve a desired formation with the same but possibly time-varying angular velocity vectors [2, 4]. Quaternion-based hybrid feedback control strategies were proposed on SO(3) for a single rigid body [5] or for a network of rigid bodies [6] where the communication architecture was selected in the form of a serial network. The translational motion control in the formation control of multi-agent systems is investigated in many papers such as [2, 3, 7–9] where the double integrator dynamics are used to represent the dynamics of the system. Some of these papers considered different consensus scenarios such as leaderless consensus, consensus regulation, and consensus tracking [10] and some considered uncertainties in the dynamics model [11, 12]. Decentralized optimal position control is studied in [13] for multi-spacecraft formation where communication between controllers and

estimators are considered in the presence of measurement uncertainties. On the other hand, attitude control of rigid body vehicles is investigated separately in several other papers such as [14].

Time delays arise due to communication delays between agents in a networks in the measurement, or processing delays including delays which occur in the actuators. A few authors have studied delayed feedback control design for formation control in the case that the current states are unavailable for feedback. Consensus problems in multi-agent systems with time delay have been considered in the sense of translational control [8, 9], attitude control [14–16], or consensus problem of multi-agent systems in general [17] with input and/or communication delays for different communication topologies. The formation control of both translational and rotational motion is a more challenging problem, specifically when the coupled dynamics are considered, and despite the importance of this topic, few studies have been dedicated to it. In [4], both the translational and rotational dynamics were considered where the equations were assumed to be decoupled. In order to consider coupled dynamics, the problem of geometric consensus of multi-agents should be defined on the nonlinear manifold of the Lie group SE(3) as in [18–23]. A survey of the work on geometric consensus theory was provided in [24] where the linear consensus algorithms were extended to nonlinear consensus resulting in global convergence properties. A Lyapunov-based feedback control law was designed on the Lie group of rigid body motions SE(3) in [23] to attain desired translational and rotational motions of spacecraft where the relative equations of each spacecraft were written with respect to a virtual leader and a collision avoidance scheme was implemented to ensure collision-free operations.

In this paper, the decentralized position and attitude consensus problem of a multi-agent spacecraft formation with time delay in the communication links between the agents is studied, where each vehicle is modeled as a rigid body and the communication architecture is modeled as a digraph. Therefore, due to time delay which cannot be avoided or ignored, the current states are unlikely to be available for state feedback. The time delay is assumed to be constant and the same in all communication links between the agents. The purpose of control is for the spacecraft, each modeled as a rigid body, to achieve attitude synchronization while they maintain a desired

distance with respect to each other. However, only the relative configurations of the spacecraft are considered and hence the formation at the desired configuration may have non-zero inertial angular and translational velocities. The problem of formation control on the Lie group SE(3) is converted to the stabilization problem of the error dynamics containing relative velocities and exponential coordinates associated with the linear space of the Lie algebra $\mathfrak{se}(3)$ for two cases: (a) circular orbits and (b) elliptic orbits. The closed-loop error dynamics are in the form of a set of time-invariant DDEs and time-periodic DDEs in cases (a) and (b), respectively. In the first case, the characteristic equation is used to study stability of the system in the frequency domain. In the second case, however, the matrix of coefficients is time periodic and hence infinite dimensional Floquet theory is used for stability analysis of the system.

The implementation on Lie groups enables the treatment of coupled rotational and translational dynamics and hence results in more accurate results compared to the case of considering decoupled dynamics for translational and rotational motions. More importantly, this formulation allows for directly treating control inputs in the body frames of vehicles, without the necessity of doing coordinate frame transformations between inertial and body frames. A tetrahedron-shaped 4-vehicle formation is considered as an example to demonstrate the successful application of the method to establishment and maintenance of relative positions and attitudes.

The paper is organized as follows. In Section 2, some preliminaries on graph theory are given and the mathematical formulation in Lie groups in general is introduced. The formation control on SE(3) is given in Section 3. The stability of consensus is studied in Section 4 for the two cases of circular and elliptical orbits. In Section 5, the fourth order Runge Kutta integration scheme used in the numerical simulations is introduced to illustrate the time update of the translational and rotational infinitesimal displacements. The numerical simulation results are then given in Section 6. Concluding remarks and discussions are presented in Section 7.

2 Mathematical Model

2.1 Communication architecture

It is desired to control the position and attitude of N rigid multi-agent spacecraft in neighboring orbits to a specified consensus state consisting of synchronized attitudes and predetermined relative positions. The communication architecture is such that the digraph $\mathcal{G}$ associated with the formation is strongly connected. This is a standard assumption for digraphs where every pair of separate vertices are connected through a directed path [25,26]. The general scheme of the problem is given in Fig. 1 in the case of $N = 4$ with each spacecraft of arbitrary orientation indicated by a small square-head line located at each vertex. It is assumed that, due to communication time

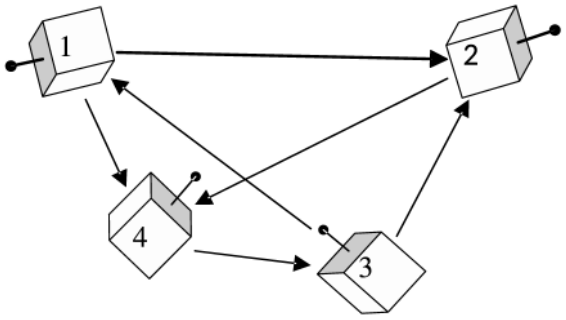

Figure 1: Digraph of the communication architecture between the four spacecraft.

delay, the current relative states are not available for state feedback. Here, the time delay is assumed to be known, time-invariant, and identical in all communication links between the spacecraft which is the same situation as in [14,27], although the approach introduced here may be extended to the case of unknown (constant) communication delay with a known upper bound.

The incidence function $\psi_{\mathcal{G}}$ of the (directed) graph $\mathcal{G}$ indicates how the vertices are connected through the (directed) edges of the graph. The communication topology can be described by the adjacency matrix $A = [a_{ij}] \in \mathbb{R}^{N\times N}$ where $a_{ij} = 1$ if the ordered pair of vertices (i, j) is contained in the incidence function $\psi_{\mathcal{G}}$, i.e. $\psi_{\mathcal{G}}(e) = (i, j)$ [28] where i is the tail of the edge e and j is its head. Otherwise, $a_{ij} = 0$. Note that by convention, the tail i of the arrow receives information from the head j of the arrow. This is written as $i \sim j$ to denote that i and j are neighbors. In addition, the degree matrix and normalized adjacency matrix are defined in the

following, which will be used to characterize the type of formation. Let d_i, $i = 1, 2, \cdots, N$, be the degree of each vertex (spacecraft) in the digraph. In the physical sense, d_i is the number of spacecraft that spacecraft i receives information from (e.g. $d_1 = 2$ for the communication architecture shown in Fig. 1). The degree matrix D is defined as $D = \text{diag}([d_i]) \in \mathbb{R}^{N\times N}$, $i = 1, 2, \cdots, N$, and the normalized adjacency matrix is defined as $\bar{A} = D^{-1}A$ [14]. Then, the adjacency matrix, degree matrix, and normalized adjacency matrix associated to the decentralized formation shown in Fig. 1 are obtained as

$$A = \begin{bmatrix} 0 & 1 & 0 & 1 \\ 0 & 0 & 0 & 1 \\ 1 & 1 & 0 & 0 \\ 0 & 0 & 1 & 0 \end{bmatrix}, \quad D = \text{diag}([2, 1, 2, 1]), \quad \bar{A} = \begin{bmatrix} 0 & \frac{1}{2} & 0 & \frac{1}{2} \\ 0 & 0 & 0 & 1 \\ \frac{1}{2} & \frac{1}{2} & 0 & 0 \\ 0 & 0 & 1 & 0 \end{bmatrix}. \tag{1}$$

For a formation associated with a digraph, the type of formation can be characterized in the sense of being centralized or decentralized based on the eigenvalues of $\bar{A}$ as described in the following. For a decentralized or leaderless formation, 1 is a simple eigenvalue of $\bar{A}$ while the rest of the eigenvalues are inside or on the unit circle [2, 29]. This can be verified by solving for the eigenvalues of $\bar{A}$ in Eq. (1), as examined in [14]. For a centralized or leader-follower type of formation, however, at least one of the eigenvalues of $\bar{A}$ is zero (because of a zero row in A). Furthermore, if the digraph associated with the formation is acyclic, i.e. no directed circles can be found in the digraph, then it can be shown that the algebraic and geometric means of the eigenvalues of the matrix $I_N + A$ (where $I_N \in \mathbb{R}^{N\times N}$ is the identity matrix of the same size as A) are equal and hence all eigenvalues of $I_N + A$ are equal to 1 [30]. Therefore, since the eigenvalues of A are shifted from those of $I_N + A$ by 1, all eigenvalues of A (and $\bar{A}$) are zero. Note that if the digraph associated with a formation is acyclic, then that formation is automatically leader-follower. This can be verified by drawing acyclic digraphs with certain number of vertices and trying all the possibilities and see that for each acyclic digraph, there is always at least one vertex with all arrows going towards that vertex. Then, that vertex represents the leader associated with that digraph, since all other vertices receive information from

it, and hence the formation is centralized.

2.2 System formulation on Lie group

The configuration (i.e. position and attitude) of each spacecraft can be represented by an element g of the Lie group SE(3), i.e. (also known as Denavit-Hartenberg representation of configuration in robotics)

$$g = \begin{bmatrix} R & r \\ 0_{1\times 3} & 1 \end{bmatrix} \in \mathrm{SE}(3), \tag{2}$$

where $R \in \mathrm{SO}(3)$ is the rotation matrix from the spacecraft body frame to the inertial frame and $r \in \mathbb{R}^3$ is the position vector from the origin of the Earth-centered inertial (ECI) frame to the center of mass of the spacecraft expressed in the inertial frame. Due to the geometric structure of the nonlinear manifold SE(3), the state space is not diffeomorphic to a vector space. Note that the spacecraft index is suppressed in this section. The augmented velocity vector of each spacecraft is

$$V = [\omega^T, v^T]^T \in \mathbb{R}^6, \tag{3}$$

where $\omega \in \mathbb{R}^3$ and $v \in \mathbb{R}^3$ denote the inertial angular and translational velocities, respectively, expressed in the body frame of the spacecraft. According to Eqs. (2) and (3), the state of each spacecraft can be represented by $(g, V) \in \mathrm{SE}(3) \times \mathbb{R}^6 = \mathrm{TSE}(3)$, the tangent bundle of SE(3). Now, using the coupled equations, the position and attitude can be considered simultaneously, and hence control design in SE(3) is more versatile compared to the techniques that consider the translational and attitude dynamics separately, particularly when translational/rotational coupling is present.

A set of mappings required to express the dynamics in a compact form are defined in the following.

Definition 1. The adjoint action map is defined for $g = g(R, r) \in \mathrm{SE}(3)$ as

$$\mathrm{Ad}_g = \begin{bmatrix} R & 0_{3\times 3} \\ r^{\times} R & R \end{bmatrix} \in \mathbb{R}^{6\times 6}, \tag{4}$$

where, for $\Omega \in \mathbb{R}^3$,

$$\Omega^\times = \begin{bmatrix} 0 & -\Omega_3 & \Omega_2 \\ \Omega_3 & 0 & -\Omega_1 \\ -\Omega_2 & \Omega_1 & 0 \end{bmatrix} \in \mathfrak{so}(3) \tag{5}$$

and the space of 3×3 real skew-symmetric matrices is denoted by $\mathfrak{so}(3)$, the Lie algebra of the Lie group SO(3), such that $\mathbf{e}_1^\times \mathbf{e}_2 = \mathbf{e}_1 \times \mathbf{e}_2$ for $\mathbf{e}_1, \mathbf{e}_2 \in \mathbb{R}^3$.

Definition 2. The adjoint operator ad_V is defined for $V = [\omega^T,\ v^T]^T \in \mathbb{R}^6$ as

$$\mathrm{ad}_V = \begin{bmatrix} \omega^\times & 0_{3\times3} \\ v^\times & \omega^\times \end{bmatrix} \in \mathbb{R}^{6\times6} \tag{6}$$

and the co-adjoint operator is defined as

$$\mathrm{ad}_V^* = \mathrm{ad}_V^T = \begin{bmatrix} -\omega^\times & -v^\times \\ 0_{3\times3} & -\omega^\times \end{bmatrix}. \tag{7}$$

Definition 3. The wedge map $(.)^\vee :\ \mathbb{R}^6 \to \mathfrak{se}(3)$ is defined for $V = [\omega^T,\ v^T]^T \in \mathbb{R}^6$ as

$$V^\vee = \begin{bmatrix} \omega^\times & v \\ 0_{1\times3} & 0 \end{bmatrix} \in \mathfrak{se}(3). \tag{8}$$

Hence, $\mathbb{R}^6$ is isomorphic to the Lie algebra $\mathfrak{se}(3)$ of SE(3).

3 Formation Control on Lie Group

The kinematic and kinetic equations of motion of spacecraft i with respect to the inertial frame expressed in the body frame of spacecraft i can be written as

$$\dot{g}_i = g_i V_i^\vee \tag{9a}$$

$$\dot{V}_i = \mathbb{I}_i^{-1}\mathrm{ad}_{V_i}^* \mathbb{I}_i V_i + \mathbb{I}_i^{-1} u_i + \mathbb{I}_i^{-1} u_i^g, \tag{9b}$$

$$(g_i(\eta), V_i(\eta)) = \phi_i(\eta), \quad -\tau \le \eta \le 0, \tag{9c}$$

where all the states are time dependent. In Eq. (9), u_i denotes the delayed consensus algorithm to be introduced, τ represents the time delay, $\phi(.)$ is the history function (necessary to define the initial value problem since delayed feedback will be used), and the tensor of mass (m_i) and inertia (J_i) properties is

$$\mathbb{I}_i = \begin{bmatrix} J_i & 0_{3\times3} \\ 0_{3\times3} & m_i I_3 \end{bmatrix} \in \mathbb{R}^{6\times6}. \tag{10}$$

In Eq. (9), u_i^g represents the gravity gradient forces and moments applied to each spacecraft with the effects of J_2 perturbation. This gravity effect can be represented as

$$u_i^g = \begin{bmatrix} M_i^g \\ F_i^g + m_i R_i^T a_i^{J_2} \end{bmatrix} \tag{11}$$

where the gravity gradient force and moment are obtained as

$$\begin{aligned} F_i^g = &\quad -\frac{m_i\mu_i}{\|r_i\|^3}\left[I_3 + \frac{3}{m_i\|r_i\|^2}\left(\frac{1}{2}\mathrm{tr}(J_i)I_3 + J_i - \frac{5}{2}\frac{r_i^T R_i J_i R_i^T r_i}{\|r_i\|^2} I_3\right)\right] R_i^T r_i, \\ M_i^g = &\quad \frac{3\mu}{\|r_i\|^5}(R_i^T r_i)^\times J_i R_i^T r_i \end{aligned} \tag{12}$$

and the acceleration due to J_2 is [23]

$$a_i^{J_2} = -\frac{3\mu J_2 R_E^2}{2\|r_i\|^5}\begin{bmatrix} (r_i\cdot\hat{I})\left(1 - \frac{5(r_i\cdot\hat{K})^2}{\|r_i\|^2}\right) \\ (r_i\cdot\hat{J})\left(1 - \frac{5(r_i\cdot\hat{K})^2}{\|r_i\|^2}\right) \\ (r_i\cdot\hat{K})\left(3 - \frac{5(r_i\cdot\hat{K})^2}{\|r_i\|^2}\right) \end{bmatrix} \tag{13}$$

where $(\hat{I}, \hat{J}, \hat{K})$ is the unit basis of the inertial frame, R_E is the Earth's radius, and μ is the gravitational parameter of the Earth.

The relative velocity of spacecraft i with respect to spacecraft j expressed in the body frame of spacecraft i is

$$V_{i/j} = V_i - \mathrm{Ad}_{g_{i/j}^{-1}} V_j, \quad (i, j = 1, 2, \cdots, N), \tag{14}$$

where $g_{i/j}$ denotes the relative configuration of spacecraft i with respect to spacecraft j and can be obtained as

$$g_{i/j} = g_j^{-1} g_i. \tag{15}$$

Note it can be easily shown that if $g_i, g_j \in \mathrm{SE}(3)$, then $g_{i/j} \in \mathrm{SE}(3)$.

Let the desired constant relative configuration between spacecraft i and spacecraft j be defined as

$$g_{i/j}^d = \begin{bmatrix} I_3 & r_{i/j}^d \\ 0_{1\times 3} & 1 \end{bmatrix}, \quad (i, j = 1, 2, \cdots, N). \tag{16}$$

The relative configuration tracking error between each two spacecraft that are connected in the digraph is expressed by the exponential coordinates

$$X_{i/j} = \left[\log_{\mathrm{SE}(3)} \left((g_{i/j}^d)^{-1} g_{i/j}\right)\right]^{|}, \quad (i, j = 1, 2, \cdots, N) \tag{17}$$

where $(.)^{|} : \mathfrak{se}(3) \to \mathbb{R}^6$ is the inverse mapping of $(.)^{\vee}$ and $\log_{\mathrm{SE}(3)} : \mathrm{SE}(3) \to \mathfrak{se}(3)$ is the logarithm map, i.e. the inverse of the exponential map $\exp : \mathfrak{se}(3) \to \mathrm{SE}(3)$, and is defined as

$$\log_{\mathrm{SE}(3)}(g) = \begin{bmatrix} \Theta^{\times} & p \\ 0_{1\times 3} & 0 \end{bmatrix} \in \mathfrak{se}(3), \tag{18}$$

where Θ is the principal rotation vector such that

$$\Theta^{\times} = \log_{\mathrm{SO}(3)}(R) = \begin{cases} 0, & \theta = 0, \\ \frac{\theta}{2\sin\theta}(R - R^T), & \theta \in (-\pi, \pi),\ \theta \neq 0, \end{cases} \tag{19}$$

where $\theta = \|\Theta\| = \cos^{-1}[\frac{1}{2}(\mathrm{tr}(R) - 1)]$, with singularity at $\theta = \pi$, and $p = S^{-1}(\Theta) r$ where the matrix S is defined as

$$S(\Theta) = I + \tfrac{1-\cos\theta}{\theta^2}\Theta^{\times} + \tfrac{\theta - \sin\theta}{\theta^3}\left(\Theta^{\times}\right)^2. \tag{20}$$

Note that the relative exponential coordinates of the spacecraft configuration $X_{i/j} = [\Theta_{i/j}^T, p_{i/j}^T]^T$ is composed of the relative principal rotation vector $\Theta_{i/j}$ and $p_{i/j} = S^{-1}(\Theta) r_{i/j}$ where $r_{i/j}$ is the relative translational displacement. When the relative configuration $g_{i/j}(t)$ approaches the desired configuration $g_{i/j}^d$, the relative configuration exponential tracking error, represented by the exponential coordinates, goes to zero and the desired formation between the spacecraft is achieved. Furthermore, when the exponential coordinates go to zero, according to Eq. (18), the relative configuration $g_{i/j}$ approaches the desired configuration. Due to the singularity at $\theta = \pi$ in Eq. (18), the controller designed based on the local stability analysis results in the desired configuration as long as the initial principal rotation angle is less than π radians. Note that equivalent Taylor series expansion should be used for small principal rotation angles.

The spacecraft are required to achieve a consensus in terms of maintaining a desired distance with respect to each other and achieving attitude synchronization. However, only the relative (not inertial) configurations of the spacecraft are considered and hence the spacecraft formation may have an arbitrary inertial angular and translational velocity as well as independent synchronized angular velocities of the spacecraft. Hence the consensus state cannot be considered as a single rigid body moving in space. To elaborate, after the consensus is achieved, the geometric frame formed by the N spacecraft remains constant in shape and moves with respect to the inertial frame with the translation and angular velocity required to maintain on the orbit. However the spacecraft at the corners of the geometric frame may rotate with respect to that frame while their relative translational velocities remain zero and they have negligible relative angular velocities. When the motion of the set of spacecraft is not committed to be in a predefined format relative to the inertial frame or, more generally, relative to a reference (which is the case in the centralized formation), more fuel efficiency may be achieved [14, 31].

On the other hand, delay is unavoidable in the communication links as shown in [16, 32–37] and hence the current states are unlikely to be available for state feedback. Therefore, a delayed consensus law is investigated in this work to simulate the more realistic situation.

Therefore, the decentralized delayed consensus algorithm with a constant delay is proposed for spacecraft i $(i = 1, 2, \cdots, N)$ as

$$u_i(t) = -(KI_6 + \mathrm{ad}^*_{V_i(t)})\mathbb{I}_i V_i(t) - \mathbb{I}_i \sum_{k=1}^{d_i} a_{i/k} \left[\Lambda X_{i/k}(t-\tau) + \Gamma \dot{X}_{i/k}(t-\tau)\right] \tag{21}$$

where τ is the time delay in the communication links in the digraph corresponding to formation, $a_{i/k} = \frac{1}{d_i}$ if spacecraft i receives data from spacecraft k, i.e. $i \sim k$, and is zero otherwise, $K > 0$ is a scalar, and Λ and Γ are 6×6 diagonal control gain matrices. The first three diagonal elements of matrices Λ and Γ are scalars λ_t and γ_t which correspond to the rotational dynamics and the second three diagonal elements of these matrices are scalars λ_f and γ_f which correspond to the translational dynamics.

According to Eq. (21), none of the spacecraft are considered to be leaders, since all connections between the spacecraft are considered in the control law. That is, as long as spacecraft i receives data from spacecraft k, their relative configurations is taken into account in the consensus design. Therefore, as opposed to [23], there is no need to have the dynamics of a (virtual) leader in this approach, provided that the communications graph is strongly connected, and hence the consensus control is decentralized. The closed-loop dynamics of the system is therefore represented by Eqs. (9), (11), (14), (15), and (21). The tracking error dynamics are obtained by substituting the expressions for $V_{i/j}$ and $X_{i/j}$ in Eqs. (14) and (17) into the kinematic and kinetic equations of motion given in Eq. (9) to yield

$$\dot{X}_{i/j}(t) = B(X_{i/j}(t))V_{i/j}(t) \tag{22a}$$

$$\dot{V}_{i/j}(t) = \dot{V}_i(t) + \mathrm{ad}_{V_{i/j}(t)}\mathrm{Ad}_{g^{-1}_{i/j}(t)}V_j(t) - \mathrm{Ad}_{g^{-1}_{i/j}(t)}\dot{V}_j(t), \quad (i, j = 1, 2, \cdots, N) \tag{22b}$$

where the fact that $\frac{d}{dt}\left(\mathrm{Ad}_{g^{-1}_{i/j}(t)}\right) = -\mathrm{ad}_{V_{i/j}(t)}\mathrm{Ad}_{g^{-1}_{i/j}(t)}$ is used to obtain Eq. (22b) from Eq. (14). In Eq. (22a), the B operator is obtained from the infinite series expansion given in terms of the Bernoulli numbers and can be expressed in the compact form

for $X = [\Theta^T, p^T]^T$ as [38]

$$B(X) = \left(I_3 + \frac{1}{2}\mathrm{ad}_X + F_1(\theta)\mathrm{ad}_X^2 + F_2(\theta)\mathrm{ad}_X^4 \right) \tag{23}$$

where

$$\begin{aligned} F_1(\theta) &= \tfrac{2}{\theta^2} - \tfrac{3}{4\theta}\ \cot\left(\tfrac{\theta}{2}\right) - \tfrac{1}{8}\ \csc^2\left(\tfrac{\theta}{2}\right) \\ F_2(\theta) &= \tfrac{1}{\theta^4} - \tfrac{1}{4\theta^3}\ \cot\left(\tfrac{\theta}{2}\right) - \tfrac{1}{8\theta^2}\ \csc^2\left(\tfrac{\theta}{2}\right) \end{aligned} \tag{24}$$

and θ is given in Eq. (19). Note that $\dot{V}_i$ in Eq. (22b) is obtained from Eq. (9b) and hence the dynamics in Eq. (22) include the gravity effects given in Eq. (11).

The control goal can then be expressed as

$$\lim_{t\to\infty} \left(X_{i/j}(t), V_{i/j}(t) \right) = (0,0) \in \mathbb{R}^{C_2^N} \times \mathbb{R}^{C_2^N}, \tag{25}$$

where C_2^N denotes the number of different combinations of N spacecraft, 2 at a time, without repetitions, i.e. N choose 2. Using Eq. (14) and the fact that $\mathrm{ad}_{\mathcal{X}}\mathcal{X} = 0$, it can be shown that

$$\mathrm{ad}_{V_{i/j}}\mathrm{Ad}_{g_{i/j}^{-1}} V_j = \mathrm{ad}_{V_{i/j}} V_i. \tag{26}$$

Substituting the consensus protocol given in Eq. (21) into Eq. (9b), substituting the result into Eq. (22b), and using Eq. (26) yields

$$\begin{aligned} \dot{V}_{i/j}(t) = \quad & -\sum_k a_{i/k} \left[\Lambda X_{i/k}(t-\tau) + \Gamma B(X_{i/k}(t-\tau)) V_{i/k}(t-\tau) \right] + \mathrm{ad}_{V_{i/j}(t)} V_i(t) + \\ & \mathrm{Ad}_{g_{i/j}^{-1}}(t) \sum_k a_{j/k} \left[\Lambda X_{j/k}(t-\tau) + \Gamma B(X_{j/k}(t-\tau)) V_{j/k}(t-\tau) \right] - K V_{i/j}(t). \end{aligned} \tag{27}$$

Taking time derivative of both sides of kinematics in Eq. (22a) and substituting Eq. (27) into the resulted ordinary differential equation (ODE), the tracking error

dynamics is obtained as

$$\begin{aligned}\ddot{X}_{i/j}(t) = \quad & \left(\dot{B}(X_{i/j}(t))B^{-1}(X_{i/j}(t)) - K\right)\dot{X}_{i/j}(t) + \\ & B(X_{i/j})(t)\left(\mathrm{ad}_{V_{i/j}}V_i(t) - \sum_{k=1}^{d_i} a_{i/k}\left(\Lambda X_{i/k}(t-\tau) + \Gamma\dot{X}_{i/j}(t-\tau)\right) + \right. \\ & \left.\mathrm{Ad}_{g_{i/j}^{-1}(t)}\sum_{k=1}^{d_j} a_{j/k}\left(\Lambda X_{j/k}(t-\tau) + \Gamma\dot{X}_{i/j}(t-\tau)\right)\right) \end{aligned} \tag{28}$$

which is a nonlinear delayed differential equation (DDE).

In the stability analysis, we are more interested in the behavior of dynamical system as the time goes to infinity. At this point, the consensus is defined such that the angular velocities (and translational velocities) of the agents are almost the same since the stability is asymptotic. Therefore, the linearization about the origin is possible. Using the Taylor expansions for $B(X_{i/j})$ and $B^{-1}(X_{i/j})$ and the property of the adjoint function, $\mathrm{ad}_{\mathcal{X}}\mathcal{Y} = -\mathrm{ad}_{\mathcal{Y}}\mathcal{X}$, and after some manipulations the closed-loop dynamics (28) can be linearized about the origin as (see the appendix)

$$\dot{X}(t) = G(t)X(t) + HX(t-\tau) \tag{29}$$

where the augmented state vector X for a strongly connected communication architecture is defined such that it consists of $2C_2^N$ vectors each of size 6×1: C_2^N vectors in the form of X_{j_1/j_2} ($j_1 = 1, 2, \cdots, N-1$, $j_2 = j_1+1, j_1+2, \cdots, N$) and C_2^N vectors being the time derivatives of the first C_2^N vectors. The matrices $G(t)$ and H in Eq. (29) are

$$G(t) = \begin{bmatrix} 0_{6C_2^N\times 6C_2^N} & I_{6C_2^N} \\ 0_{6C_2^N\times 6C_2^N} & -G_{22}(t) \end{bmatrix}, \quad H = \begin{bmatrix} 0_{6C_2^N\times 6C_2^N} & 0_{6C_2^N\times 6C_2^N} \\ -H_{21}\mathcal{C} & -H_{22}\mathcal{C} \end{bmatrix}, \tag{30}$$

where

$$G_{22}(t) = KI_{C_2^N} + \mathrm{blkdiag}\left(\mathrm{ad}_{V(t)}\right) \tag{31}$$

and H_{21} and H_{22} are $6C_2^N \times 6C_2^N$ block diagonal matrices constructed from 6×6

matrices Λ and Γ, respectively. In Eq. (31), blkdiag(ad_V) denotes a block diagonal matrix constructed from $(N-1)$ matrices of the form $\mathrm{ad}_{V_1}(t)$, $(N-2)$ matrices of the form $\mathrm{ad}_{V_2}(t)$, $\cdots$, $(N-j)$ matrices of the form $\mathrm{ad}_{V_j}(t)$, $\cdots$, 2 matrices of the form $\mathrm{ad}_{V_{N-2}(t)}$, and the matrix $\mathrm{ad}_{V_{N-1}(t)}$ (overall, a block diagonal of C_2^N matrices each of the size 6×6).

According to the definition above, the X vector for the case of four spacecraft is in the form of $X = \left[X_{1/2}^T, X_{1/3}^T, X_{1/4}^T, X_{2/3}^T, X_{2/4}^T, X_{3/4}^T, \dot{X}_{1/2}^T, \dot{X}_{1/3}^T, \dot{X}_{1/4}^T, \dot{X}_{2/3}^T, \dot{X}_{2/4}^T, \dot{X}_{3/4}^T\right]^T$. The $\mathcal{C}$ matrix for this case can be expressed in general as

$$\mathcal{C} = \begin{bmatrix} (\frac{s_{21}}{d_2} - \frac{s_{12}}{d_1})I_6 & \frac{s_{13}}{d_1}I_6 & \frac{s_{14}}{d_1}I_6 & \frac{s_{23}}{d_2}Q_{1/2} & \frac{s_{24}}{d_2}Q_{1/2} & 0_{6\times6} \\ -\frac{s_{12}}{d_1}I_6 & (\frac{s_{13}}{d_1} - \frac{s_{31}}{d_3})I_6 & -\frac{s_{14}}{d_1}I_6 & \frac{s_{32}}{d_3}Q_{1/2} & 0_{6\times6} & \frac{s_{34}}{d_3}Q_{1/3} \\ -\frac{s_{12}}{d_1}I_6 & -\frac{s_{13}}{d_3}I_6 & (\frac{s_{41}}{d_4} - \frac{s_{14}}{d_1})I_6 & 0_{6\times6} & -\frac{s_{42}}{d_4}Q_{1/2} & -\frac{s_{43}}{d_4}Q_{1/3} \\ \frac{s_{21}}{d_2}Q_{2/1} & -\frac{s_{31}}{d_3}Q_{2/1} & 0_{6\times6} & (\frac{s_{23}}{d_2} - \frac{s_{32}}{d_3})I_6 & \frac{s_{24}}{d_2}I_6 & \frac{s_{34}}{d_3}Q_{2/3} \\ \frac{s_{21}}{d_2}Q_{2/1} & 0_{6\times6} & -\frac{s_{41}}{d_4}Q_{2/1} & -\frac{s_{23}}{d_2}I_6 & (\frac{s_{42}}{d_4} - \frac{s_{24}}{d_2})I_6 & -\frac{s_{43}}{d_4}Q_{2/3} \\ 0_{6\times6} & \frac{s_{31}}{d_3}Q_{3/1} & -\frac{s_{41}}{d_4}Q_{3/1} & \frac{s_{32}}{d_3}Q_{3/2} & -\frac{s_{42}}{d_4}Q_{3/2} & (\frac{s_{34}}{d_3} - \frac{s_{43}}{d_4})I_6 \end{bmatrix} \quad (32)$$

where

$$Q_{i/j} = I_6 - \begin{bmatrix} 0_{3\times3} & 0_{3\times3} \\ \left(r_{i/j}^d\right)^\times & 0_{3\times3} \end{bmatrix} \quad (33)$$

and $s_{ij} = 1$ if spacecraft i receives data from spacecraft j, i.e. $i \sim j$, and $s_{ij} = 0$ otherwise. Since $s_{ij} = 0$ implies that $s_{ji} \neq 0$ or vice versa for directed graph, there is always more than 6 zeros in the matrix $\mathcal{C}$. Furthermore, there is always more than one zero in every row of $\mathcal{C}$ for the case of a leaderless graph. Note that the relative exponential coordinate $X_{i/j}$ is expressed in the body frame of spacecraft i and hence the mapping $X_{i/j} = \mathrm{Ad}_{g_{i/k}^{-1}} X_{k/l}$ holds. More specifically, for the communication

architecture under study (see Fig. 1), the $\mathcal{C}$ matrix becomes

$$\mathcal{C} = \begin{bmatrix} -\frac{1}{2}I_6 & 0_{6\times6} & \frac{1}{2}I_6 & 0_{6\times6} & Q_{1/2} & 0_{6\times6} \\ -\frac{1}{2}I_6 & -\frac{1}{2}I_6 & -\frac{1}{2}I_6 & \frac{1}{2}Q_{1/2} & 0_{6\times6} & 0_{6\times6} \\ -\frac{1}{2}I_6 & 0_{6\times6} & -\frac{1}{2}I_6 & 0_{6\times6} & 0_{6\times6} & -Q_{1/3} \\ 0_{6\times6} & -\frac{1}{2}Q_{1/2} & 0_{6\times6} & -\frac{1}{2}I_6 & I_6 & 0_{6\times6} \\ 0_{6\times6} & 0_{6\times6} & 0_{6\times6} & 0_{6\times6} & -I_6 & -Q_{2/3} \\ 0_{6\times6} & \frac{1}{2}Q_{3/1} & 0_{6\times6} & \frac{1}{2}Q_{3/2} & 0_{6\times6} & -I_{6\times6} \end{bmatrix}. \tag{34}$$

4 Stability Analysis

In this section, the local stability of the closed-loop dynamics is studied using the linearized system of Eq. (29) for two cases: a) circular orbits and b) elliptic orbits. Equation (29) is in the form of a set of linear time-invariant DDEs and time-periodic DDEs in cases (a) and (b), respectively. In the first case, the characteristic equation can be used to study stability of the system in the frequency domain. In the second case, however, infinite dimensional Floquet theory needs to be implemented for stability analysis of the system.

4.1 Stability analysis in the case of a circular orbit

In this case, the velocities of the spacecraft (V_i, $i = 1, 2, \cdots, N$) can be approximated as the constant circular orbital velocity since the orders of the spacecraft relative velocities (and the spacecraft velocities relative to a nearby circular orbit) are much less than the circular velocity itself. Hence, G_{22} in Eq. (29) is nearly a constant matrix and characteristic equation of the linearized system in Eq. (29) can be written as

$$\begin{aligned} &\det\left(sI_{12C_2^N} - G - He^{-\tau s}\right) = \\ &\qquad \det(sI_{6C_2^N})\det\left(sI_{6C_2^N} + G_{22} + \left(H_{22} + \frac{H_{21}}{s}\right)e^{-\tau s}\mathcal{C}\right) = 0. \end{aligned} \tag{35}$$

Remark 1. According to the determinant of partitioned matrices, the characteristic

equation in Eq. (35) for $s = 0$ becomes

$$\begin{aligned}\det(-G-H) = &\quad \det\left(\begin{bmatrix} 0_{6C_2^N\times 6C_2^N} & -I_{6C_2^N} \\ H_{21}\mathcal{C} & G_{22}+H_{22}\mathcal{C}\end{bmatrix}\right)\\ = &\quad \det(G_{22}+H_{22}\mathcal{C})\det((G_{22}+H_{22}\mathcal{C})^{-1}H_{21}\mathcal{C})\\ = &\quad \det(H_{21}\mathcal{C}). \end{aligned} \tag{36}$$

For the communication architecture shown in Fig. 1, the determinant of the matrix $\mathcal{C}$ given in Eq. (34) is nonzero and since H_{21} is diagonal, $\det(H_{21}\mathcal{C}) \neq 0$. Therefore, $s = 0$ is not a root for the characteristic equation in Eq. (35). □

According to Remark 1, the characteristic equation in Eq. (35) can be written as

$$\det\left(sI_{6C_2^N} + G_{22} + \left(H_{22} + \frac{H_{21}}{s}\right)e^{-\tau s}\mathcal{C}\right) = 0 \tag{37}$$

and after multiplying both sides of Eq. (37) by $s^{C_2^N}$ (recall that $s = 0$ is not a root of the characteristic equation when $H_{21} \neq 0$) and using Eq. (31), the former becomes

$$\det\left(s^2 I_{6C_2^N} + KIs + \text{blkdiag}(\text{ad}_V)s + (H_{22}s + H_{21})\,e^{-\tau s}\mathcal{C}\right) = 0. \tag{38}$$

The system becomes unstable when the eigenvalues leave the left half complex plane. The exponential polynomial in Eq. (38) is of the order of $12C_2^N$ and the stability condition cannot be obtained parametrically in the general case. Therefore, some assumptions need to be made to study stability in the system.

Remark 2. If one assumes that the delayed exponential coordinates and their time derivatives are not included in the feedback, i.e. $H_{21} = 0$ and $H_{22} = 0$, then the characteristic equation (38) can be expressed as

$$\prod_{l=1}^{6C_2^N}(s + K + s_{b_l}) = 0, \tag{39}$$

where s_{b_l} $(l = 1, 2, \cdots, 6C_2^N)$ are eigenvalues of $\text{blkdiag}(\text{ad}_V)$. Any of the factors of polynomial in the conservative characteristic equation in this case can be expressed

as

$$s + K + s_{b_l} = 0. \tag{40}$$

Therefore, in order for the system with no delayed feedback to be stable, it suffices that

$$K > \rho_1 \tag{41}$$

where

$$\rho_1 = \max(\|s_{b_l}\|), \qquad l = 1, 2, \cdots, 6C_2^N. \tag{42}$$

Besides, using a symbolic toolbox, it can be shown that, for the communication architecture represented by the matrix $\mathcal{C}$, the characteristic equation given in Eq. (38) of the linearized system is independent of the translational velocities of the spacecraft. Therefore, provided that the norm of the angular velocities are small (as will be seen in the simulation results), the stability can be studied based on the characteristic equation with either H_{21} or H_{22} being zero. For $H_{21} = 0$ and $H_{22} \neq 0$, the characteristic equation can be approximated as

$$\prod_{l=1}^{C_2^N} \left(s + K + \gamma e^{-\tau s} s_{\mathcal{C}_l}\right) = 0. \tag{43}$$

where $s_{\mathcal{C}_l}$ $(l = 1, 2, \cdots, 6C_2^N)$ are eigenvalues of $\mathcal{C}$ and, without loss of generality,

$$\gamma = \max(|\gamma_t|, |\gamma_f|) \tag{44}$$

is used.

Any of the factors of polynomial in the characteristic equation in this case can be expressed as

$$s + K + \gamma e^{-\tau s} s_{\mathcal{C}_l} = 0 \tag{45}$$

To investigate stability, the imaginary axis crossings should be studied. As described before, $s = 0$ is not a root for the characteristic equation. Hence, s is assumed to be in the imaginary form of $s = j\omega$. Then, the (complex) eigenvalue of $\mathcal{C}$, $s_{\mathcal{C}_l}$, is written in the polar form and is substituted into Eq. (45) with $s = j\omega$. Separating the real and imaginary parts and some algebra, ω^2 is obtained as

$$\omega^2 = \gamma^2 \|s_{\mathcal{C}_l}\|^2 - K^2. \tag{46}$$

If there is a real solution for ω, it implies that the eigenvalues of the system cross the imaginary axis and, as a result, the system becomes unstable. Therefore, in order for the system to be stable, ω needs to be either imaginary or complex. Hence, according to Eq. (46),

$$K > \gamma \rho_2 \tag{47}$$

for stability, where $\rho_2 = \max(\|(s_{\mathcal{C}_l})\|)$, $(l = 1, 2, \cdots, C_2^N)$.

However, none of the assumptions above can be used in the linear stability analysis, since when $H_{21} = 0$ the determinant in Eq. (36) is no longer nonzero and hence $s = 0$ is a root of the characteristic equation. Therefore, the equilibrium becomes non-hyperbolic and nonlinear terms, given up to the quadratic order in the appendix, should also be considered in the analysis and stability should be determined based on the normal form. Therefore, the stability analysis given in this section provides only a reasonable choice of the control gains such that, based on Eqs. (41) and (47),

$$K > \rho_1 + \gamma \rho_2. \tag{48}$$

The stability of the system based on the selected control gains can then be verified by investigating the spectral radius of the monodromy matrix obtained using the method introduced in Section 4.2. □

According to Eqs. (21), when

$$\lambda = \max(|\lambda_t|, |\lambda_f|) \tag{49}$$

is zero, only the derivatives of the exponential coordinates are included in the feedback. However, it is desired for the exponential coordinates themselves to be in the feedback as well. Therefore, λ should be a small positive number. On the other hand, according to the expression for ρ_1 in Eq. (42) and due to the fact that the velocity adjoint function (ad_V) is a lower triangular matrix with diagonal block matrices being only in terms of the angular velocity components, ρ_1 is of the order of the maximum norm of the angular velocities of the spacecraft in orbit at consensus which, without loss of generality, can be assumed to be a small number. Therefore, according to Eq. (48) and what discussed above, a good choice for the control gains Λ, Γ, and K to guarantee the asymptotic stability of the closed-loop coupled translation- and attitude dynamics in the case of circular orbit is such that $K \gg \lambda > 0$ and $K \gg \gamma > 0$. A set of control gains satisfying this condition can also be used as a guess for the case of an elliptic orbit which will be presented in the simulation results.

Note that in a special case, if each agent receives information from one and only one other agent, e.g. when the communication architecture can be represented by a directed cycle graph, then the summation notation in the control law will be relaxed. Also, in the case of a centralized formation control, a feedback control law could be designed [23] based on the relative configuration of each spacecraft with respect to the (actual or virtual) chief in order to cancel the nonlinear terms of the closed-loop dynamics and achieve global asymptotic stability of the system. However, such a control law cannot be designed in the case of a decentralized control.

4.2 Stability analysis in the case of an elliptic orbit

In this case, the velocities of the spacecraft can be approximated as the time-periodic velocity of the elliptic orbit. As a result, the governing equations describing the dynamics of the system become in the form of periodic DDEs. After linearization about the equilibrium state, periodic DDE is expressed as in Eq. (29), where the $G(t)$ matrix is periodic with the period of the orbit. This can be realized from Eqs. (30) and (31) and the fact that the velocities of the agents are periodic with the period of the orbit. It can be shown that the periodic DDE in Eq. (29) can be treated as an abstract ODE [39].

In general, the abstract representation of Eq. (29) is the evolution of the history function $\boldsymbol{\phi}$ in a Banach space [39, 40], i.e.

$$\dot{\mathcal{Y}}(t) = \mathcal{A}(t)\mathcal{Y}(t), \tag{50}$$

with $\mathcal{Y}(0) = \boldsymbol{\phi}$, where the operator $\mathcal{A}(t)$ is periodic. Using a numerical method called the Chebyshev spectral continuous time approximation (CSCTA) [39], the abstract ODE representation can be approximated with a large-dimensional system of ODEs.

An infinite dimensional dynamic map can then be defined for the closed-loop system as [41]

$$m_X(i) = \mathcal{U} m_X(i-1) \tag{51}$$

that maps the state vector X in the time interval $[-T, 0]$ to that in $[0, T]$, where T is the (orbital) period, and subsequently to the other periods after that. In Eq. (51), m_X is an expansion of the state vector X in some basis which satisfies the initial condition of $m_X(0) = m_\phi$, where $\phi(.)$ is the history function and m_ϕ is the expansion of $\phi(\theta)$, and $\mathcal{U}$ is the infinite dimensional monodromy operator. All eigenvalues of $\mathcal{U}$ must lie inside the unit circle in the complex plane for the system to be stable. The stability of the closed-loop system may then be investigated in the parameter space of available control gains using Floquet theory to obtain the spectral radius of the monodromy operator which must be less than unity for asymptotic stability.

To approximate $\mathcal{U}$ by a matrix of finite dimension, the CSCTA technique is used. Note that another numerical technique that can be used to efficiently generate an approximation to the infinite-dimensional monodromy operator $\mathcal{U}$ is expansion in terms of Chebyshev polynomials as discussed in [42].

In the CSCTA method, the interval $[t-\tau, t]$ is discretized into $n = m-1$ subintervals whose unequal lengths are determined from the m Chebyshev collocation points defined on $[-1, 1]$. Chebyshev collocation points can be introduced as the projections of the equispaced points on the upper half of the unit circle onto the horizontal axis

as

$$t_\alpha = \cos\frac{\alpha\pi}{n}, \quad \alpha = 0, 1, 2, \cdots, n. \tag{52}$$

The illustration for the Chebyshev collocation points is given in Fig. 2. A Chebyshev spectral differentiation matrix D is defined as

$$\begin{aligned}
&D_{11} = \frac{2n^2+1}{6} = -D_{m,m}, \quad D_{\beta\beta} = -\frac{t_\beta}{2(1-t_\beta^2)}, \ \beta = 2, \cdots, n \\
&D_{\alpha\beta} = \frac{c_\alpha(-1)^{\alpha+1}}{c_\beta(t_\alpha - t_\beta)}, \ \alpha \neq \beta, \ \alpha, \beta = 1, 2, \cdots, m, \\
&c_\alpha = \begin{cases} 2, \ \alpha = 1, m \\ 1, \ \text{otherwise.} \end{cases}
\end{aligned} \tag{53}$$

Application of CSCTA discretizes the infinite-dimensional abstract representation of the DDE system, i.e. Eq. (50), into a $mq-$dimensional set of periodic ODEs, where $q = 12C_2^N$ ($q = 72$ when $N = 4$) is the dimension of the system in Eq. (29). That is,

$$\dot{Y}(t) = \hat{A}(t)Y(t) \tag{54}$$

where the mq-dimensional $Y(t)$ vector is expressed as

$$Y(t) \ = \left[\begin{array}{ccccc} X^T(t) & \cdots & X^{\mathrm{T}}(t-\tau) \end{array} \right]^T = \left[\begin{array}{cccccc} Y_0^T(t) & Y_1^T(t) & Y_2^T(t) & \cdots & Y_n^T(t) \end{array} \right]^T \tag{55}$$

where $Y_\alpha(t) = X\left(t - \frac{\tau}{2}(1-t_\alpha)\right)$, $\alpha = 0, 1, 2, \cdots, n$. The $mq \times mq$ time-varying matrix $\hat{A}(t)$ in Eq. (54) is expressed as

$$\hat{A}(t) = \left[\begin{array}{ccccc} G(t) & 0_{q\times q} & \cdots & 0_{q\times q} & H \\ & & \frac{2}{\tau}\left[\mathbb{D}_{mq\times mq}^{(q+1,mq)}\right] & & \end{array} \right], \tag{56}$$

where the matrices $G(t)$ and H are given in Eq. (30), $\mathbb{D}_{mq\times mq} = D_{m\times m} \otimes I_q$, and $\otimes$ is the Kronecker product. Superscript $(q+1, mq)$ on $\mathbb{D}_{mq\times mq}$ refers to the fact that only rows of $\mathbb{D}_{mq\times mq}$ between $q+1$ and mq are written into the remaining $(m-1)q \times mq$ part of matrix $\hat{A}(t)$. Note that the $2/\tau$ factor in front of the portion of $\mathbb{D}_{mq\times mq}$ above accounts for the fact of rescaling the standard collocation expansion interval $[-1, 1]$

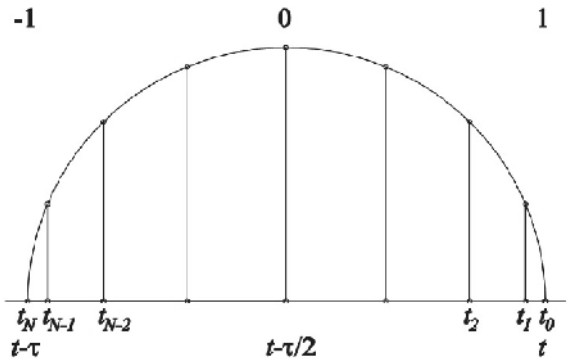

Figure 2: Chebyshev collocation points [43]

to $[0, \tau]$.

The monodromy matrix U associated with Eq. (54) is the approximation of the monodromy operator $\mathcal{U}$ introduced by Eq. (51), which is obtained by the numerical propagation of $\dot{U} = \hat{A}(t)U$ with the initial condition $U_0 = I_{mq}$. The spectral radius of the monodromy matrix associated with Eq. (54) must be less than unity in order for the closed-loop system to be locally asymptotically stable. Note that the spectral accuracy of the CSCTA technique is inherited from Chebyshev spectral collocation [44]. The exponential convergence of CSCTA is numerically verified in [39].

5 Integration Scheme of the Delayed Consensus

In this section, an integration scheme is developed that will further be used in the simulation results. Due to time delay in the communication links, the effects of time delay should be considered when developing the integration scheme. More details on the Runge-Kutta technique that accommodates time delay in the systems can be found in [45,46]. Furthermore, the evolution of the rotation matrices requires a careful treatment when integrating the states of the system. Therefore, any integration scheme used for the system under study must account for both time delay and the evolution of the rotation matrices. Note that due to the evolution of the rotation matrices, the MATLAB `dde23` integrator cannot be applied for such system. However, the delayed fourth-order Runge-Kutta integration scheme proposed here accounts for both time delay and rotation matrices.

Let the $\oplus$ operator be defined such that when applied to two variables a and b, i.e. $a \oplus b$, it preserves the set to which those variables belong. Also, let δt be the

time step and h and $\hat{h}$ be the nearest integers to ${}^{t_h}/_{\delta t}$ and ${}^{\tau}/_{\delta t}$, respectively, such that for $h \leq \hat{h}$ (i.e. $t_h \leq \tau$) the history function $\phi(\eta)$, $-\tau \leq \eta \leq 0$, needs to be used to evaluate the states (g, V) at time $(h - \hat{h})\delta t \approx t_h - \tau$.

The operator $\oplus$ is equivalent to a summation when used for any variables other than the rotation matrix, including the augmented velocity vector $V = [\omega^T, v^T]^T$ and the displacement vector r. For rotation-type elements of the configuration (i.e. $R_h \oplus \delta R_h$), however, the $\oplus$ operator acts as described in the following. The angular velocity ω_h at time t_h is first extracted from velocity vector V_h at time t_h. Then, the infinitesimal principal rotation $\delta\Theta_h$ at time t_h is used in the Rodriguez formula as

$$\delta R_h = \exp_{\mathrm{SO}(3)}(\delta\Theta_h) = I + \frac{\sin\delta\theta_h}{\delta\theta_h}\delta\Theta_h^{\times} + \frac{1-\cos\delta\theta_h}{\delta\theta_h^2}\left(\delta\Theta_h^{\times}\right)^2, \tag{57}$$

where $\delta\theta_h = \|\delta\Theta_h\| = \omega_h\delta t$ is the infinitesimal principal rotation angle at time t_h, to obtain the infinitesimal rotation matrix δR_h at the corresponding time step. The time-updated rotation matrix is then obtained as $R_{h+1} = R_h\delta R_h$. Note that likewise the non-rotational terms, the rotation matrix is also iterated four times at each time interval using a new iterated value of the angular velocity as described above. Furthermore, since (g, V) and $(\delta g, \delta V)$ are members of $\mathrm{SE}(3) \times \mathbb{R}^6$, according to the aforementioned properties of the $\oplus$ operator,

$$(g, V) \oplus (\delta g, \delta V) \in \mathrm{SE}(3) \times \mathbb{R}^6 \tag{58}$$

and

$$g \oplus \delta g = \begin{bmatrix} R\delta R & r + \delta r \\ 0_{1\times 3} & 1 \end{bmatrix}, \quad V \oplus \delta V = V + \delta V. \tag{59}$$

Therefore, the states of the system at the $(h+1)$th time step can be obtained in terms of those at the hth time step as

$$(g_{h+1}, V_{h+1}) = (g_h, V_h) \oplus \frac{1}{6}\left(k_{1,h} + 2k_{2,h} + 2k_{3,h} + k_{4,h}\right)\delta t \tag{60}$$

where

$$
\begin{aligned}
k_{1,h} &= f\left(t_h, \quad (g_h, V_h), \quad (g_{h-\hat{h}}, V_{h-\hat{h}})\right), \\
k_{2,h} &= f\left(t_h + \frac{\delta t}{2}, \quad (g_h, V_h) \oplus \frac{k_{1,h}}{2}, \quad (g_{h-\hat{h}}, V_{h-\hat{h}}) \oplus \frac{k_{1,h-\hat{h}}}{2}\right), \\
k_{3,h} &= f\left(t_h + \frac{\delta t}{2}, \quad (g_h, V_h) \oplus \frac{k_{2,h}}{2}, \quad (g_{h-\hat{h}}, V_{h-\hat{h}}) \oplus \frac{k_{2,h-\hat{h}}}{2}\right), \\
k_{4,h} &= f\left(t_h + \delta t, \quad (g_h, V_h) \oplus k_{3,h}, \quad (g_{h-\hat{h}}, V_{h-\hat{h}}) \oplus k_{3,h-\hat{h}}\right),
\end{aligned} \tag{61}
$$

and where f denotes the dynamics of the system given in Eq. (9). k_1, k_2, k_3, and k_4 at each time step are therefore arrays containing elements of $(\delta g, \delta V)$-type.

It can be realized from Eqs. (9) and (21) that the governing equations of the closed-loop dynamics form a set of retarded DDEs. Therefore, the method of steps can be followed confidently without much concern about the possibility of discontinuity growth. The method of steps converts each DDE to a sequence of ODEs as described in the following. In this method, the time is divided into intervals of length τ as $[0, \tau]$, $[\tau, 2\tau]$, etc. Then, in each time interval, the DDE is written in the form of an ODE such that all time derivatives and functions of the current states form the homogeneous part of that ODE and the delayed terms are replaced with the solution of the ODE corresponding to the previous time interval to construct the nonhomogeneous part of the current ODE. For more details about this method, the reader is referred to [47].

As mentioned before, the extended Runge-Kutta integration scheme introduced in this section accounts not only for the time delay but also for the evolution of the rotation matrix, which is mandatory when rotation matrices are considered as the attitude parametrization set. In addition, because of the order of integration, the integration scheme proposed in this section is more accurate than, for instance, forward difference integration. To the authors knowledge, this is the first time that such a scheme is developed for formation control on SE(3) including time delay in the system. This integration scheme is further used in the numerical simulations.

Table 1: Initial displacement (km) and velocity (m/s) deviations of spacecraft with respect to the periapsis of the Molniya orbit.

$r_{1/M}$	$r_{2/M}$	$r_{3/M}$	$r_{4/M}$
$\begin{bmatrix} 3.7532 \\ 1.9249 \\ -4.0549 \end{bmatrix}$	$\begin{bmatrix} -0.8635 \\ -0.5206 \\ 2.0701 \end{bmatrix}$	$\begin{bmatrix} -0.1334 \\ 5.5692 \\ 3.1424 \end{bmatrix}$	$\begin{bmatrix} -7.1323 \\ 1.1558 \\ 0.7080 \end{bmatrix}$
$v_{1/M}$	$v_{2/M}$	$v_{3/M}$	$v_{4/M}$
$\begin{bmatrix} 45 \\ -15 \\ -42 \end{bmatrix}$	$\begin{bmatrix} -263 \\ -125 \\ -136 \end{bmatrix}$	$\begin{bmatrix} 60 \\ 80 \\ 37 \end{bmatrix}$	$\begin{bmatrix} 260 \\ 120 \\ -137 \end{bmatrix}$

6 Simulation Results

Four mircosatellites ($N = 4$) each of mass 60 kg and inertia tensor of

$$J = \begin{bmatrix} 4.97 & 0 & 0 \\ 0 & 6.16 & 0 \\ 0 & 0 & 8.37 \end{bmatrix} \text{ kg.m}^2 \tag{62}$$

are assumed to be in moderate proximity in neighboring Earth orbits which are in the neighborhood of a Molniya orbit. The initial deviations of each spacecraft expressed in the ECI frame are given in Table 1 with respect to the periapsis of the Molniya orbit. The body frame of each spacecraft is initially assumed to be aligned with its drag frame. That is, the x–axis of the body frame of each spacecraft is initially in the direction of its velocity vector, the z–axis is normal to the orbital plane of the spacecraft orbit, and the y–axis is obtained from the right hand rule.

The desired formation configuration is selected such that the four spacecraft construct a tetrahedron-shaped formation of 1 km edge length such that the coordinates of the four spacecraft are given in a "tetrahedron frame"as

$$(0,0,0), \quad (-1,0,0), \quad \left(-\frac{1}{2}, \frac{\sqrt{3}}{2}, 0\right), \quad \left(-\frac{1}{2}, \frac{\sqrt{3}}{6}, \sqrt{\frac{2}{3}}\right).$$

The communication delay is selected as $\tau = 1$ s. The history function is selected to

be constant and is equal to $\phi = (g_0, V_0)$ where g_0 and V_0 are chosen as

$$g_1(t_0) = \begin{bmatrix} 0.7956 & -0.2435 & 0.5547 & 3650.2 \\ 0.6053 & 0.2839 & -0.7436 & -2826.9 \\ 0.0236 & 0.9274 & 0.3733 & -5651.2 \\ 0 & 0 & 0 & 1 \end{bmatrix}, \quad g_2(t_0) = \begin{bmatrix} 0.3770 & -0.0928 & 0.9215 & 3645.2 \\ 0.9113 & 0.2150 & -0.3512 & -2830.4 \\ -0.1655 & 0.9722 & 0.1656 & -5646.0 \\ 0 & 0 & 0 & 1 \end{bmatrix}$$

$$g_3(t_0) = \begin{bmatrix} -0.1160 & 0.1075 & 0.9874 & 3645.6 \\ 0.9695 & 0.2282 & 0.0890 & -2824.3 \\ -0.2158 & 0.9677 & -0.1307 & -5644.6 \\ 0 & 0 & 0 & 1 \end{bmatrix}, \quad g_4(t_0) = \begin{bmatrix} -0.5754 & 0.2821 & 0.7677 & 3640.8 \\ 0.8012 & 0.3830 & 0.4598 & -2829.2 \\ -0.1643 & 0.8796 & -0.4464 & -5648.6 \\ 0 & 0 & 0 & 1 \end{bmatrix} \tag{63a}$$

$$V_1(t_0) = [0,\ 0,\ 0.0150,\ 9.7572,\ 0,\ 0]^T, \quad V_2(t_0) = [0,\ 0,\ 0.0145,\ 9.4509,\ 0,\ 0]^T$$

$$V_3(t_0) = [0,\ 0,\ 0.0111,\ 9.7724,\ 0,\ 0]^T, \quad V_4(t_0) = [0,\ 0,\ 0.0075,\ 9.9737,\ 0,\ 0]^T \tag{63b}$$

where expressions for g and V are given in Eqs. (2) and (3), the displacements are in km, the velocities are in km/s, and angular velocities are in rad/s. In Eq. (63), the initial orientations of the spacecraft 2-4 are assumed to be different from the initial orientation of spacecraft 1 through 3-1-3 Euler angles $[\pi/12, \pi/12, \pi/12]$, $[\pi/6, \pi/6, \pi/6]$, and $[\pi/4, \pi/4, \pi/4]$, respectively. Furthermore, given the initial translational deviations of the spacecraft in Eq. (63), the initial linear velocities of the spacecraft are chosen as in Eq. (63b) to be consistent with the dynamics of each spacecraft on its orbit. As mentioned before, the x–axis of the body frame of each spacecraft is initially in the direction of its translational velocity vector. Therefore, the initial angular velocities are obtained as $\omega_{i0} = \dot{\nu}_{i0} - \dot{\phi}_{i0_{fpa}}$ $(i = 1, 2, 3, 4)$, where ν_{i0} and $\phi_{i0_{fpa}}$ denote the the initial true anomaly and flight path angle of spacecraft i. Using Eqs. (2.93) and (2.94) in [48] and the relation between the angular momentum magnitude and the rate of true anomaly ($\dot{\nu}_i = h_i / r_i^2$), the initial angular velocity norms are obtained as

$$\|\omega_{0i}\| = \frac{h_i}{r_i^2} \frac{1 + e_i \cos \nu_i}{1 + 2e_i \cos \nu_i + e_i^2}, \tag{64}$$

where e_i denotes the eccentricity of the orbit of spacecraft i.

In the consensus problem, it is important for the error dynamics of the rotational and translational motion to become zero almost at the same amount of time. To satisfy this requirement, the elements of the control gain matrices Λ and Γ are selected as $\lambda_t = \gamma_t = 0.08$ and $\lambda_f = \gamma_f = 0.02$. Furthermore, according to the numerical simulations, $\rho_1 = 0.0390\,\text{rad/s}$ and $\rho_2 = 6.2668$ (which is the determinant of the $\mathcal{C}$ matrix in Eq. (34)). Also, according to Eq. (48) and as discussed at the end of Section 4.1, the control gain K is set to be $K = 1$ to satisfy the stability condition given in Eq. (48).

The spectral radius of the monodromy matrix associated with Eq. (54) obtained by the CSCTA technique with 5 Chebyshev collocation points and time step $\Delta t = 10$s for the aforementioned system parameters and control gains is $\rho = 5.6980 \times 10^{-6}$ which is less than 1 and hence the system is locally asymptotically stable. Note that the size of the $\hat{A}(t)$ matrix in Eq. (56) for $q = 72$ and $m = 5$ is 360×360. Also note that the spectral radius for a more circular orbit is less than that of a more elliptic orbit with the same semimajor axis. For instance, the spectral radius obtained for a circular orbit of the same semimajor axis as the Molniya orbit, i.e. $a \approx 27078$ km, is obtained as $\rho = 2.9943 \times 10^{-6}$.

The relative positions of the spacecraft with respect to the Molniya orbit are shown in Figs. 3 and 4 in the ECI and local vertical local horizontal (LVLH) frames, respectively, where the asterisk $*$ denotes the location of the periapsis of the Molniya orbit at the initial epoch in the left panel of the figure while it denotes the location on that orbit at the time the tetrahedron consensus is achieved in right panel, the circle $\circ$ denotes the location of the vehicles at the periapsis of the Molniya orbit, and the cross $\times$ denotes their location when the desired configuration is achieved. The 3-dimensional relative configuration (displacement and attitude) is shown in Fig. 5 in the LVLH frame of one spacecraft which indicates that not only are the desired relative displacements achieved, but also all spacecraft have the same attitude at the desired configuration. The 2-dimensional relative displacements are shown in Fig. 6 with respect to the body frame of each spacecraft where the corresponding spacecraft can be identified by having the same initial $\bigcirc$ and final $\times$ positions in its own body frame. Relative displacements in only the last 10% of the elapsed time are shown

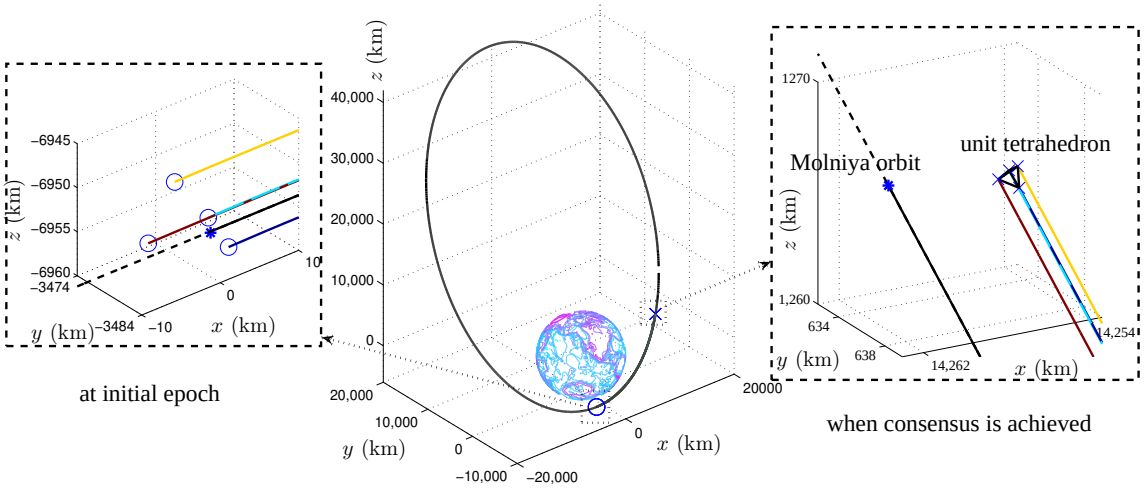

Figure 3: Relative positions of the spacecraft formation with respect to the Molniya orbit in the ECI frame at the initial epoch and after consensus is achieved.

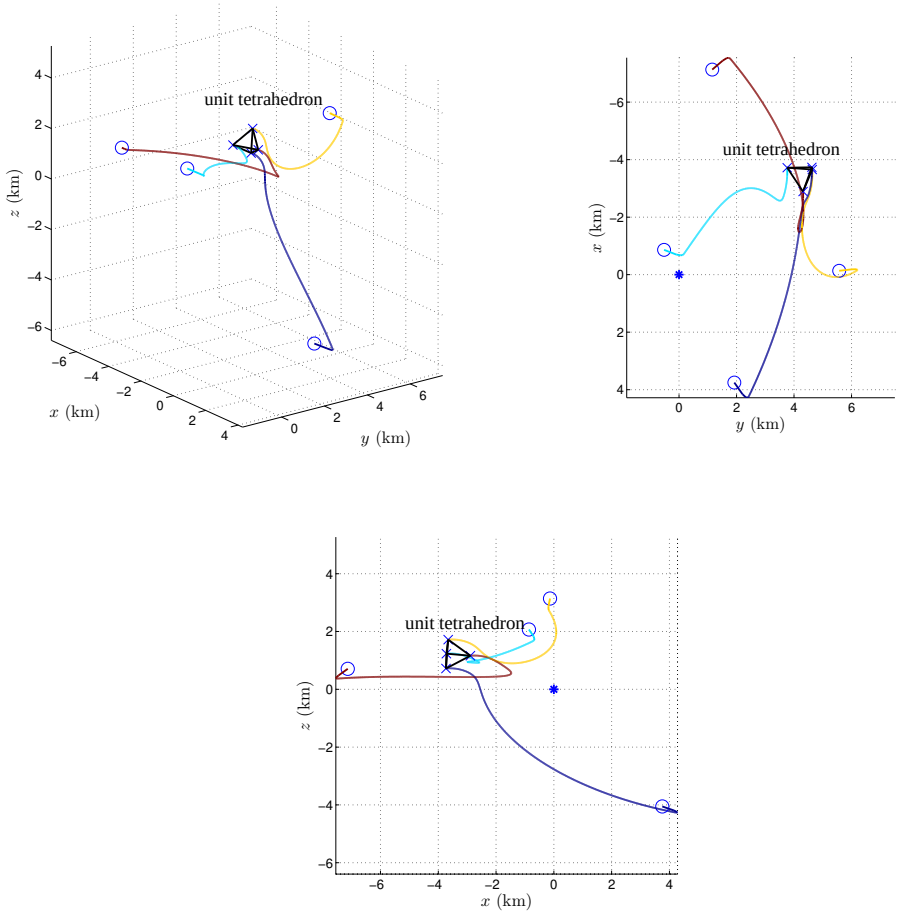

Figure 4: Positions of the spacecraft formation with respect to the Molniya orbit in the LVLH frame. The asterisk $*$ remains on the Molniya orbit.

in Fig. 7 where the black tetrahedron (with each spacecraft at each corner) in each panel is the desired relative position shown in the body frame of the corresponding spacecraft. Note that the desired position is shaped in the common $x-y$ plane of the body frame of the spacecraft. Note that the consensus tetrahedron shown in Figs. 3-6

corresponds to the time when the consensus is achieved. The consensus tetrahedron is not stationary in any of the frames used in these figures, including the spacecraft body frames since they are free to rotate independently of the tetrahedron.

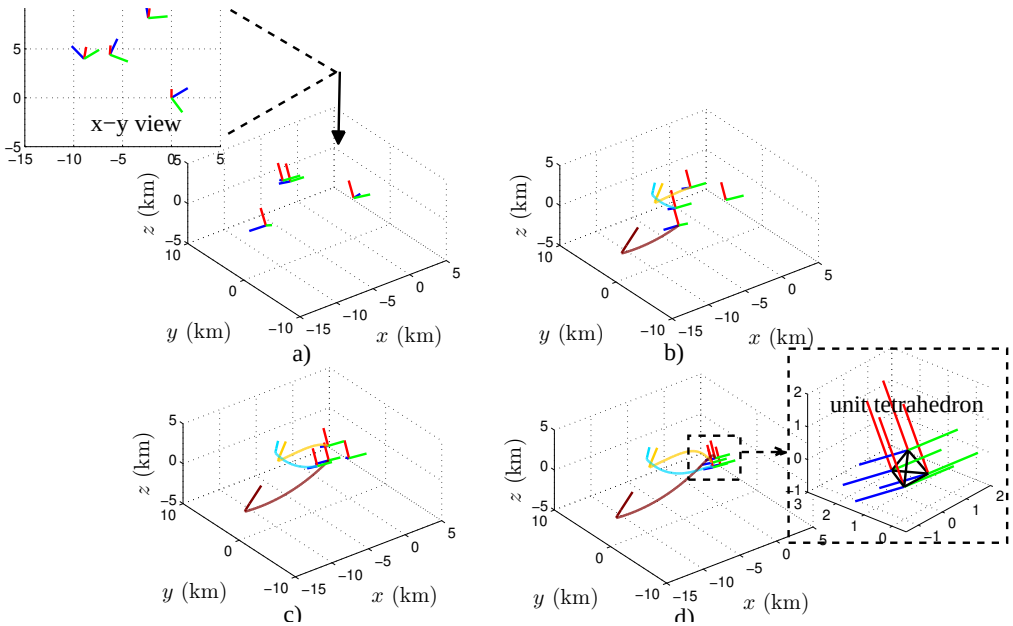

Figure 5: Relative positions and attitudes of the formation shown in the LVLH frame of one of the spacecraft a) at the initial time, b) after 5 percent of the final time, c) after 10 percent of the final time, and d) at the final time where consensus is achieved.

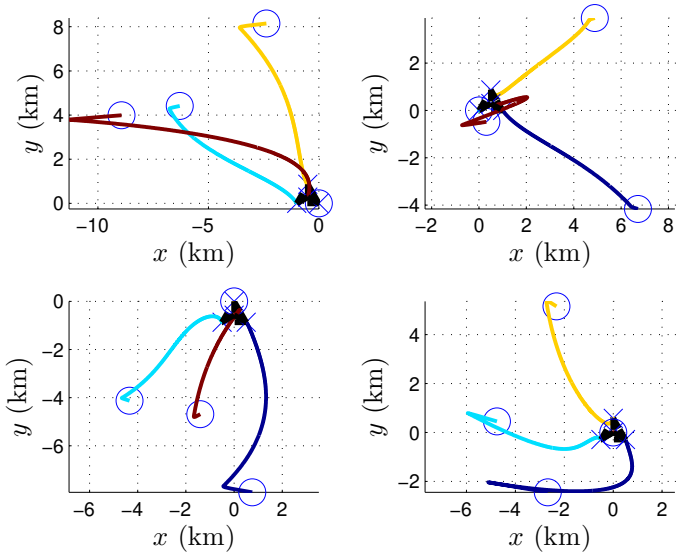

Figure 6: Relative positions of the formation with respect to the body frame of each spacecraft.

The time history of relative position with respect to one spacecraft is shown in Fig. 8. Note that all three curves approach the desired 1 km separation distance. The translational and angular velocity norms for the four spacecraft are plotted in

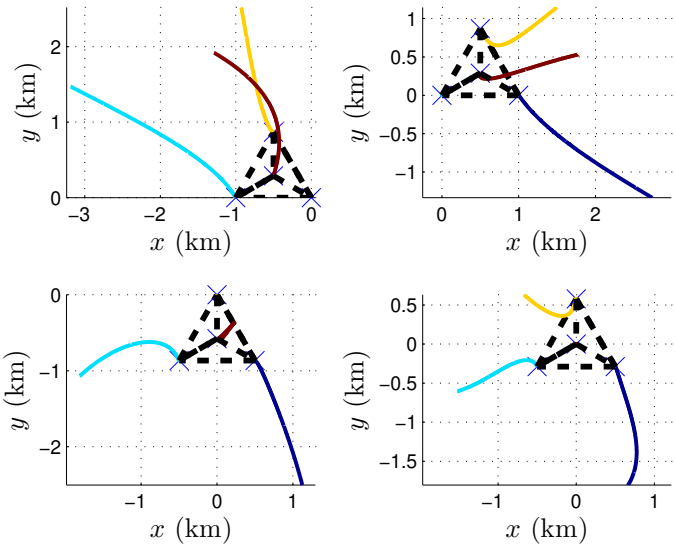

Figure 7: Relative position of the formation with respect to the body frame of each spacecraft with the transient response omitted.

Fig. 9. Note that in order for the formation to have a constant configuration, there may exist a slight difference between the translational velocities in the ECI frame. Furthermore, the *absolute* angular velocity of the spacecraft may not necessarily be zero at the desired formation. The norm of error dynamics of the system are shown in Fig. 10 in terms of the translational and angular velocities/positions. The numerical

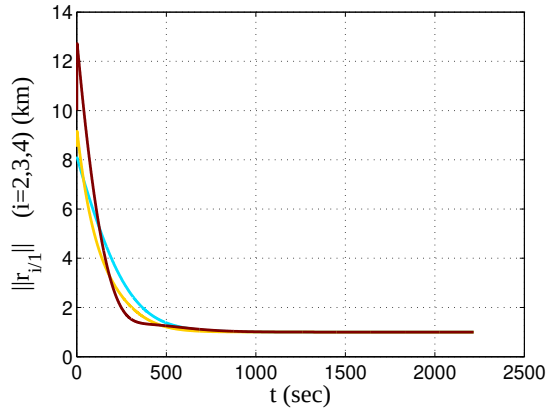

Figure 8: Norms of the relative positions of the formation with respect to one of the spacecraft.

value for ω_{0i} from Eq. (64) is of the order of 0.001 rad/s or less. However, in order to check the validity of the local stability analyses given in Section 4, the initial angular velocity norms for the four spacecraft are assumed to be 0.015, 0.0145, 0.0111, and 0.0075 rad/s (Eq. (63b)), i.e. much greater than what the spacecraft experience in reality. The initial relative angular velocities are then obtained from Eq. (14) at

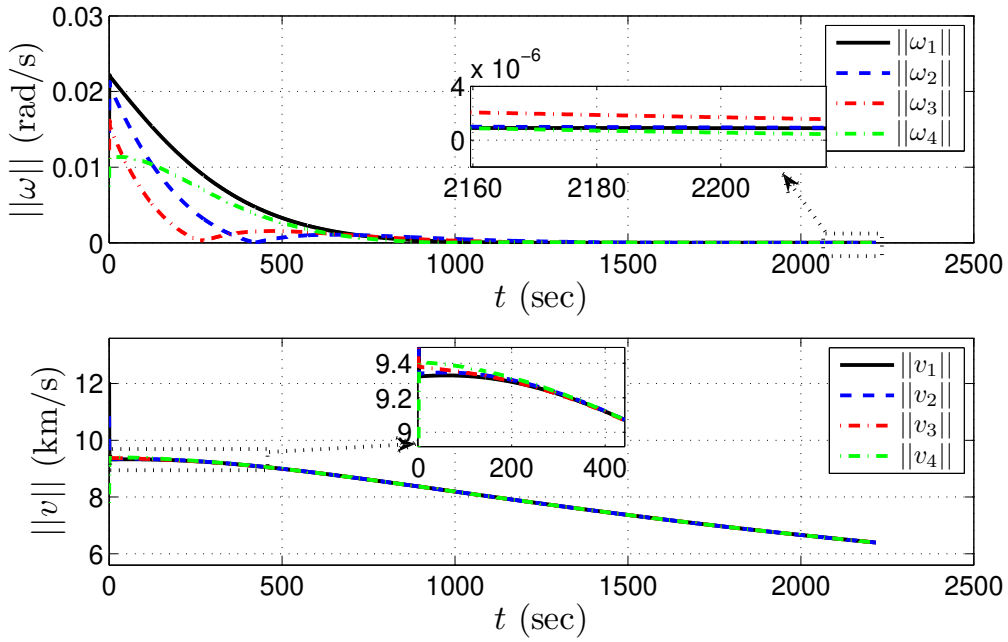

Figure 9: Norms of the translational and angular velocities of each spacecraft.

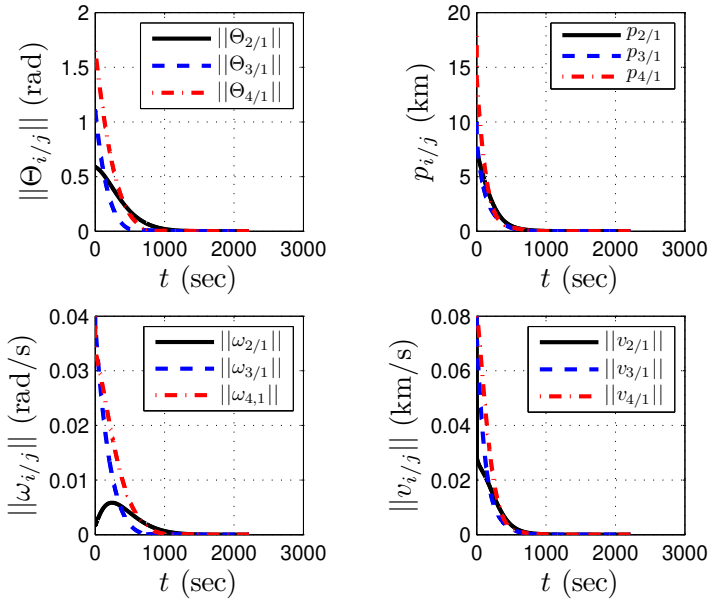

Figure 10: Relative translational and angular displacement error dynamics in terms of the exponential coordinates (top row) and relative velocity tracking errors (bottom row).

$t = 0$ as to be about 0.03 rad/s or less. According to the numerical simulations, the proposed consensus deigned based on the linearized system would still be capable of stabilizing the nonlinear system if the initial angular velocities were selected to be as large as about 0.04 rad/s, which correspond to initial relative angular velocities of about 0.08 rad/s.

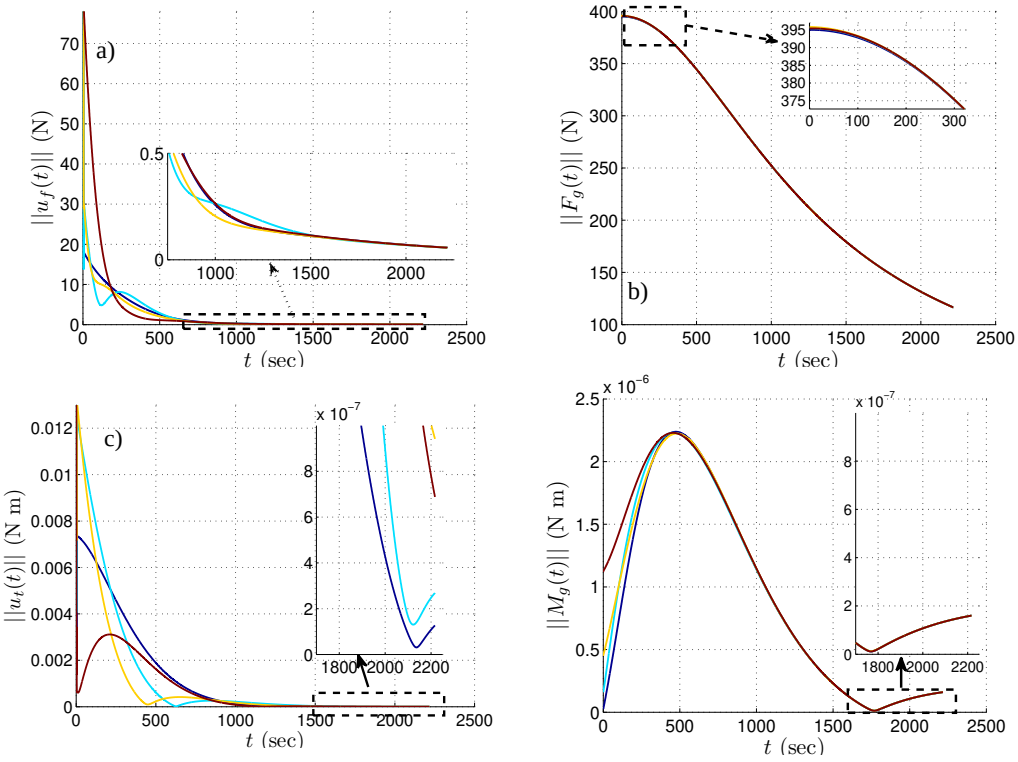

Figure 11: Norms of a) control force, b) gravity force, c) control torques, and d) gravity gradient torque for all four spacecraft.

The control force, gravity force (including J_2 and inertia effects), control torque, and gravity gradient torque applied to each spacecraft are shown in Fig. 11. According to the figure, the norm of the steady state control torque applied to one spacecraft is less than the norm of the gravity gradient torque while those applied to other spacecraft is greater than the norm of the gravity gradient moment. Furthermore, at around $t = 1770$ s the norm of the gravity gradient torque is minimum which indicates that the body frames of the spacecraft are almost aligned with the LVLH frame at this point. Note that the control forces and moments do not vanish when consensus is achieved. The reason is that they should still compensate for the gravity gradient moments and the natural tendency of the spacecraft to drift apart due to being in different orbits.

7 Conclusion

In in paper, the decentralized leaderless spacecraft consensus was studied where a constant time delay was assumed in the communication links. Each spacecraft was assumed as a rigid body and the Lie group SE(3) was used to model the coupled

translational and rotational dynamics of the spacecraft. To model the tracking error, exponential coordinates were used. The desired relative pose was defined as all spacecraft pointing to the same direction at all times while having a desired constant relative position with respect to each other. The use of SE(3) simplifies the controller design by allowing one control law to be obtained for translational and rotational motions, despite the presence of rotational/translational coupling terms.

The proof of local asymptotic stability was provided for two cases of circular and elliptic orbits by the use of exponential coordinates. In the case of a circular orbit, the error dynamics of the system are in the form of time invariant delay differential equations (DDEs) and hence stability was studied in the frequency domain to obtain a conservative characteristic exponential polynomial of the controlled system. Then, by the investigation of the imaginary axis crossings of the eigenvalues of that characteristic equation, stability conditions were obtained in terms of the control gains. In the case of an elliptic orbit, the error dynamics are in the form of time periodic DDEs and the linearized equations must be treated using infinite dimensional Floquet theory to guarantee local asymptotic stability. The numerical method of Chebyshev spectral continuous time approximation was then used for the discretization of the abstract ODE representation of the error dynamics.

In a simulation of four spacecraft in the neighborhood of the Molniya orbit, the proposed controller was able to bring the spacecraft to the desired relative pose which included a tetrahedron formation for the translational motion while the relative attitudes of the spacecraft were zero. Note that the absolute positions and attitudes of the four spacecraft were not constrained, and that the attitudes were not synchronized with the tetrahedron so that the final formation is not a rigid body. This choice was made since, according to the literature on decentralized control, when the absolute motions of the spacecraft in formation are not committed to be restricted, greater efficiency in terms of control effort may be achieved.

References

[1] K. T. Alfriend, S. R. Vadali, P. Gurfil, J. How, and L. Breger. *Spacecraft Formation Flying: Dynamics, Control, and Navigation.* Elsevier, 2009, pp. 1–12.

[2] W. Ren and Y.-Q. Chen. Leaderless Formation Control for Multiple Autonomous Vehicles. *AIAA Guidance, Navigation, and Control Conference and Exhibit, Keystone, Colorado, Paper No. AIAA 2006–6069*, 21–24 August 2006.

[3] L. A. Weitz, J. E. Hurtado, and A. J. Sinclair. Decentralized Cooperative-Control Design for Multivehicle Formations. *Journal of Guidance, Control, and Dynamics*, 31:970–979, 2008, doi: 10.2514/1.33009.

[4] W. Ren and R. W. Beard. Decentralized Scheme for Spacecraft Formation Flying via the Virtual Structure Approach. *Journal of Guidance, Control, and Dynamics*, 27:1746–1751, 2004.

[5] C. G. Mayhew, R.G. Sanfelice, and A. R. Teel. Quaternion-Based Hybrid Control for Robust Global Attitude Tracking. *IEEE Transactions on Automatic Control*, 56:2555–2566, 2011, doi: 10.1109/TAC.2011.2108490.

[6] C. G. Mayhew, R.G. Sanfelice, J. Sheng, M. Arcak, and A. R. Teel. Quaternion-Based Hybrid Feedback for Robust Global Attitude Synchronization. *IEEE Transactions on Automatic Control*, 57:2122–2127, 2012, doi: 10.1109/TAC.2011.2180777.

[7] M. Mesbahi and F. Y. Hadaegh. Formation Flying Control of Multiple Spacecraft via Graphs, Matrix Inequalities, and Switching. *Journal of Guidance, Control, and Dynamics*, 24:369–377, 2001.

[8] Y.-P. Tian and C.-L. Liu. Consensus of Multi-Agent Systems With Diverse Input and Communication Delays. *IEEE Transactions on Automatic Control*, 53, 2008, doi: 10.1109/TAC.2008.930184.

[9] T. Yucelen and W. M. Haddad. Consensus Protocols for Networked Multi-Agent Systems with a Uniformly Continuous Quasi-Resetting Ar-

chitecture. *International Journal of Control*, 87:1716–1727, 2014, doi: 10.1080/00207179.2014.883647.

[10] Z. Meng, W. Ren, Y. Cao, and Z. You. Leaderless and Leader-Following Consensus With Communication and Input Delays Under a Directed Network Topology. *IEEE Transactions on Systems, Man, and Cybernetics – Part B: Cybernetics*, 41:75–88, 2011, doi: 10.1109/TSMCB.2010.2045891.

[11] A. Das and F. L. Lewis. Cooperative Adaptive Control for Synchronization of Second-Order Systems with Unknown Nonlinearities. *International Journal of Robust and Nonlinear Control*, 21(13):1509–1524, 2011, doi: 10.1002/rnc.1647.

[12] T. Yucelen and E. N. Johnson. Control of Multivehicle Systems in the Presence of Uncertain Dynamics. *International Journal of Control*, 86:1540–1553, 2013, doi: 10.1080/00207179.2013.790077.

[13] G. M. Belanger, S. Ananyev, J. L. Speyer, D. F. Chichka, and J. R. Carpenter. Decentralized Control of Satellite Cluster Under Limited Communication. *Journal of Guidance, Control, and Dynamics*, 29:134–145, 2006.

[14] T. H. Summers, A. Chunodkar, and M. R. Akella. Rigid Body Attitude Synchronization with Unknown Communication Time Delays. *AAS/AIAA Space Flight Mechanics Meeting, San Diego, CA, Paper No. AAS 10-176*, pages 1155–1164, February 2010.

[15] J. Zhou, G. Ma, and Q. Hu. Delay Depending Decentralized Adaptive Attitude Synchronization Tracking Control of Spacecraft Formation. *Chinese Journal of Aeronautics*, 25:406–415, 2012, doi: 10.1016/S1000-9361(11)60404-4.

[16] G. Li and L. Liu. Coordinated Multiple Spacecraft Attitude Control with Communication Time Delays and Uncertainties. *Chinese Journal of Aeronautics*, 25:698–708, 2012, doi: 10.1016/S1000-9361(11)60436-6.

[17] R. Olfati-Saber and R. M. Murray. Consensus Problems in Networks of Agents with Switching Topology and Time-Delays. *IEEE Transactions on Automatic Control*, 49:1520–1533, 2004, doi: 10.1109/TAC.2004.834113.

[18] L. Scardovi, N. Leonard, and R. Sepulchre. Stabilization of Three-Dimensional Collective Motion. *Communications in Information and Systems*, 8:473–500, 2008.

[19] A. Sarlette, S. Bonnabel, and R. Sepulchre. Coordinated Motion Design on Lie Groups. *IEEE Transactions on Automatic Control*, 55:1047–1058, 2010, doi: 10.1109/TAC.2010.2042003.

[20] Y. Liu and Z. Geng. Finite-Time Optimal Formation Control of Multi-Agent Systems on the Lie group SE(3). *International Journal of Control*, 86:1675–1686, 2013, doi: 10.1080/00207179.2013.792006.

[21] R. Dong and Z. Geng. Consensus Based Formation Control Laws for Systems on Lie Groups. *Systems & Control Letters*, 62:104–111, 2013, doi: 10.1016/j.sysconle.2012.11.005.

[22] R. Dong and Z. Geng. Consensus for Formation Control of Multi-Agent Systems. *International Journal of Robust and Nonlinear Control*, pages 1–21, 2014, doi: 10.1002/rnc.3220.

[23] D. Lee, A. K. Sanyal, and E. A. Butcher. Asymptotic Tracking Control for Spacecraft Formation Flying with Decentralized Collision Avoidance. *Journal of Guidance, Control, and Dynamics, in press*, 2014, doi: 10.2514/1.G000101.

[24] R. Sepulchre. Consensus on Nonlinear Spaces. *Annual Reviews in Control*, 35:56–64, 2011, doi: 10.1016/j.arcontrol.2011.03.003.

[25] M. Mesbahi and M. Egerstedt. *Graph Theoretic Methods in Multiagent Networks*. Princeton University Press, New Jersey, 2010, p. 21.

[26] W. Ren and R. W. Beard. *Distributed Consensus in Multi-vehicle Cooperative Control: Theory and Applications*. Springer, 2008, pp. 8–11.

[27] Y. Igarashi, T. Hatanaka, M. Fujita, and M. W. Spong. Passivity-Based Attitude Synchronization in SE(3). *IEEE Transactions on Control Systems Technology*, 17:1119–1134, 2009, doi: 10.1109/TCST.2009.2014357.

[28] J. A. Bondy and U. S. R. Murty. *Graph Theory With Applications*. Elsevier, New York, 1976, pp. 1–24.

[29] W. Ren. Distributed Attitude Alignment in Spacecraft Formation Flying. *International Journal of Adaptive Control and Signal Processing*, 21:95–113, 2007, doi: 10.1002/acs.916.

[30] B. D. McKay, F. E. Oggier, G. F. Royle, N. J. A. Sloane, I. M. Wanless, and H. S. Wilf. Acyclic Digraphs and Eigenvalues of (0,1)-Matrices. *Journal of Integer Sequences*, 7:Art.04.3.3, 2004.

[31] A. Sarlette, R. Sepulchre, and N. E. Leonard. Autonomous Rigid Body Attitude Synchronization. *Automatica*, 45:572–577, 2009, doi: 10.1016/j.automatica.2008.09.020.

[32] N. Chopra and M. W. Spong. Output Synchronization of Nonlinear Systems with Time Delay in Communication. *Proceedings of the 45th IEEE Conference on Decision & Control, San Diego, CA, USA, Paper Number FrA11.3*, pages 4986–4992, December 13-15, 2006, doi: 10.1109/CDC.2006.377258.

[33] Y. Cao and W. Ren. Multi-Agent Consensus Using Both Current and Outdated States with Fixed and Undirected Interaction. *Journal of Intelligent and Robotic Systems*, 58:95–106, 2010, doi: 10.1007/s10846-009-9337-7.

[34] Z. Wang, K. You, J. Xu, and H. Zhang. Consensus Design for Continuous-Time Multi-Agent Systems with Communication Delay. *Journal of Systems Science and Complexity*, 27:701–711, 2014.

[35] C. Somarakis and J. S. Baras. Delay-Independent Stability of Consensus Networks with Application to Flocking. *Preprints, 12th IFAC Workshop on Time Delay Systems, Ann Arbor, MI, USA*, June 28-30, 2015.

[36] H. J. Savino, F.D. Souza, and L. Pimenta. Consensus on Time-Delay Intervals in Networks of High-Order Integrator Agents. *Preprints, 12th IFAC Workshop on Time Delay Systems, Ann Arbor, MI, USA*, June 28-30, 2015.

[37] I. C. Morarescu and S.-I. Niculescu. Multi-Agent Systems with Decaying Confidence and Commensurate Time-Delays. *Preprints, 12th IFAC Workshop on Time Delay Systems, Ann Arbor, MI, USA*, June 28-30, 2015.

[38] F. Bullo and R. M. Murray. Proportional Derivative (PD) Control on the Euclidean Group. *CDS Technical Report, California Institute of Technology, Pasadena, CA, Report No. 95-010*, pages 1–47, August 1995.

[39] E.A. Butcher and O.A. Bobrenkov. On the Chebyshev Spectral Continuous Time Approximation for Constant and Periodic Delay Differential Equations. *Communications in Nonlinear Science and Numerical Simulation*, 16:1541–1554, 2011, doi: 10.1016/j.cnsns.2010.05.037.

[40] M. Nazari and E. A. Butcher and O. A. Bobrenkov. Comparison of Feedback Control Strategies for Periodic Delayed Systems. *International Journal of Dynamics and Control*, 2:102–118, 2014, doi: 10.1007/s40435-013-0053-6.

[41] E.A. Butcher and B.P. Mann. *Stability Analysis and Control of Linear Periodic Delayed Systems using Chebyshev and Temporal Finite Element Methods*, chapter invited chapter in Delay Differential Equations: Recent Advances and New Directions, ed. B. Balachandran, D. Gilsinn, and T. Kalmar-Nagy. Springer, New York, 2009, pp. 93–130.

[42] E. A. Butcher, H. Ma, E. Bueler, V. Averina, and Z. Szabo. Stability of Linear Time-Periodic Delay-Differential Equations via Chebyshev Polynomials. *International Journal for Numerical Methods in Engineering*, 59:895–922, 2004, doi: 10.1002/nme.894.

[43] O. A. Bobrenkov, M. Nazari, and E. A. Butcher. Response and Stability Analysis of Periodic Delayed Systems With Discontinuous Distributed Delay. *Journal of Computational and Nonlinear Dynamics*, 7, 2012, doi:10.1115/1.4005925.

[44] O.A. Bobrenkov. *Analysis of Periodic Systems With Time Delay via Chebyshev Spectral Collocation With Application to Milling*. PhD thesis, New Mexico State University, August 2011.

[45] E. Hairer and S. P. Nørsett. *Solving Ordinary Differential Equations I.* Springer-Verlag, Berlin, 1993, pp. 339–353.

[46] G. S. Virk. Runge kutta Method for Delay-Differential Systems. *IEEE Proceedings D (Control Theory and Applications)*, 132:119–123, 1985, doi: 10.1049/ip-d.1985.0021.

[47] L. F. Shampine and S. Thompson. *Numerical Solution of Delay Differential Equations.* chapter in Delay Differential Equations – Recent Advances and New Directions, ed. B. Balachandran, T. Kalmar-Nagy, and D. E. Gilsinn, New York, 2009, pp. 245–271.

[48] D. A. Vallado. *Fundamentals of Astrodynamics and Applications.* Space Technology Library, Microcosm Press and Springer, Hawthorne and New York, Third edition, 2007, p. 113.

Appendix

Closed-loop dynamics derivations

The closed-loop dynamics in Eq. (29) can also be expressed as

$$\dot{X}(t) = G(t)X(t) + HX(t-\tau) + \begin{bmatrix} 0_{36\times 1} \\ W(t) \end{bmatrix} + O(3) \tag{A.1}$$

where the nonlinear quadratic vector field W is

$$W(t) = \left[W_{1/2}^T(t),\, W_{1/3}^T(t),\, W_{1/4}^T(t),\, W_{2/3}^T(t),\, W_{2/4}^T(t),\, W_{3/4}^T(t)\right]^T \tag{A.2}$$

and

$$
\begin{aligned}
W_{i/j}(t) = W(X_{i/j}(t), \dot{X}_{i/j}(t)) = \quad & \frac{1}{2}\frac{d}{dt}\left(\mathrm{ad}_{X_{i/j}(t)}\right)\dot{X}_{i/j}(t) + \\
& \frac{1}{2}\left(\mathrm{ad}_{V_i(t)}\mathrm{ad}_{X_{i/j}(t)} - \mathrm{ad}_{X_{i/j}(t)}\mathrm{ad}_{V_i(t)}\right)\dot{X}_{i/j}(t) - \\
& \mathrm{ad}_{X_{i/j}(t)}\sum_{k=1}^{d_i} a_{i/k}\left(\Lambda X_{i/k}(t-\tau) + \Gamma\dot{X}_{i/k}(t-\tau)\right) + \\
& \left(\mathrm{ad}_{X_{i/j}(t)} + \begin{bmatrix} -\Theta^{\times}_{i/j} & 0_3 \\ -p^{\times}_{i/j} + \Theta^{\times}_{i/j}\left(r^d_{i/j}\right)^{\times} & -\Theta^{\times}_{i/j} \end{bmatrix}\right) \times \\
& \sum_{k=1}^{d_j} a_{j/k}\left(\Lambda X_{j/k}(t-\tau) + \Gamma\dot{X}_{j/k}(t-\tau)\right) \\
= \quad & \frac{1}{2}\frac{d}{dt}\left(\mathrm{ad}_{X_{i/j}(t)}\right)\dot{X}_{i/j}(t) + \\
& \frac{1}{2}\left(\mathrm{ad}_{V_i(t)}\mathrm{ad}_{X_{i/j}(t)} - \mathrm{ad}_{X_{i/j}(t)}\mathrm{ad}_{V_i(t)}\right)\dot{X}_{i/j}(t) - \\
& \mathrm{ad}_{X_{i/j}(t)}\sum_{k=1}^{d_i} a_{i/k}\left(\Lambda X_{i/k}(t-\tau) + \Gamma\dot{X}_{i/k}(t-\tau)\right) + \\
& \begin{bmatrix} 0_3 & 0_3 \\ \Theta^{\times}_{i/j}\left(r^d_{i/j}\right)^{\times} & 0_3 \end{bmatrix}\sum_{k=1}^{d_j} a_{j/k}\left(\Lambda X_{j/k}(t-\tau) + \right. \\
& \left.\Gamma\dot{X}_{j/k}(t-\tau)\right) \qquad\qquad (A.3)
\end{aligned}
$$

Some terms in the closed-loop dynamics (28) are investigated in details here. The inverse of the invertible matrix $B_{i/j} = B(X_{i/j})$ is

$$
\begin{aligned}
B^{-1}_{i/j} = \quad & I - \frac{1}{2}\mathrm{ad}_{X_{i/j}} + \frac{1}{4}\mathrm{ad}^2_{X_{i/j}} - F_1(\theta)\mathrm{ad}^2_{X_{i/j}} + \cdots \\
= \quad & I - \frac{1}{2}\mathrm{ad}_{X_{i/j}} + \frac{1}{4}\mathrm{ad}^2_{X_{i/j}} - \frac{1}{12}\mathrm{ad}^2_{X_{i/j}} + O(3) \qquad\qquad (A.4)
\end{aligned}
$$

Hence, keeping the quadratic terms, the first term in Eq. (28) can be expressed as

$$
\begin{aligned}
\dot{B}_{i/j}B^{-1}_{i/j}\dot{X}_{i/j} = \quad & \left(\frac{1}{2}\frac{d}{dt}(\mathrm{ad}_{X_{i/j}}) - \frac{1}{4}\frac{d}{dt}(\mathrm{ad}_{X_{i/j}})\mathrm{ad}_{X_{i/j}} - \frac{1}{12}\frac{d}{dt}\left(\mathrm{ad}^2_{X_{i/j}}\right) + O(3)\right)\dot{X}_{i/j} \\
= \quad & \frac{1}{2}\frac{d}{dt}(\mathrm{ad}_{X_{i/j}})\dot{X}_{i/j} + O(3) \qquad\qquad (A.5)
\end{aligned}
$$

Also, since the adjoint function is anti-commutative, the multiplication of the B

operator, the adjoint relative velocity, and the absolute velocity can be obtained as

$$B_{i/j}\mathrm{ad}_{V_{i/j}}V_i = -B_{i/j}\mathrm{ad}_{V_i}V_{i/j} = -B_{i/j}\mathrm{ad}_{V_i}B_{i/j}^{-1}\dot{X}_{i/j} \tag{A.6}$$

$$\begin{aligned} -B_{i/j}\mathrm{ad}_{V_i}B_{i/j}^{-1}\dot{X}_{i/j} = & -\left(I+\frac{1}{2}\mathrm{ad}_{X_{i/j}}+F_1(\theta)\mathrm{ad}_{X_{i/j}}^2+F_2(\theta)\mathrm{ad}_{X_{i/j}}^4\right)\mathrm{ad}_{V_i}\,(I- \\ & \frac{1}{2}\mathrm{ad}_{X_{i/j}}+\mathrm{ad}_{X_{i/j}}^2-F_1(\theta)\mathrm{ad}_{X_{i/j}}^2+\text{h.o.t.}\Big)\,\dot{X}_{i/j} \\ = & -\mathrm{ad}_{V_i}\dot{X}_{i/j}+\frac{1}{2}\left(\mathrm{ad}_{V_i}\mathrm{ad}_{X_{i/j}}-\mathrm{ad}_{X_{i/j}}\mathrm{ad}_{V_i}\right)\dot{X}_{i/j}+O(4) \end{aligned} \tag{A.7}$$

Furthermore, it can be shown that

$$\mathrm{Ad}_{g_{i/j}^{-1}} = \begin{bmatrix} R_{i/j}^{-1} & 0_3 \\ -R_{i/j}^{-1}r_{i/j}^{\times} & R_{i/j}^{-1} \end{bmatrix} \tag{A.8}$$

Using definition of logarithm function in SE(3) given in Eq. (18), the definition of the exponential coordinates given in Eq. (17), and Eq. (19), it can be shown that

$$R_{i/j}^{-1} = \exp(-\Theta_{i/j}^{\times})\left(R_{i/j}^{d}\right)^{-1} = I-\frac{\sin\theta}{\theta}\Theta_{i/j}^{\times}+\frac{1-\cos\theta}{\theta^2}\left(\Theta_{i/j}^{\times}\right)^2. \tag{A.9}$$

The fact that $R_{i/j}^{d} = I_3$ and

$$\begin{aligned} r_{i/j} = & S(\Theta_{i/j})p_{i/j}+r_{i/j}^{d} = p_{i/j}+\frac{1-\cos\theta}{\theta^2}\Theta_{i/j}^{\times}p_{i/j}+\frac{\theta-\sin\theta}{\theta^3}\left(\Theta_{i/j}^{\times}\right)^2 p_{i/j}+ \\ & r_{i/j}^{d} \end{aligned} \tag{A.10}$$

are also used to obtain Eq. (A.9). Therefore, the Adjoint function can be implicitly expressed in terms of the exponential coordinates as

$$\begin{aligned} \mathrm{Ad}_{g_{i/j}^{-1}} = & \begin{bmatrix} I & 0_3 \\ -\left(r_{i/j}^{d}\right)^{\times} & I \end{bmatrix}+ \\ & \begin{bmatrix} -\Theta_{i/j}^{\times}+\frac{1}{2}\left(\Theta_{i/j}^{\times}\right)^2 & 0_3 \\ -p_{i/j}^{\times}+\Theta_{i/j}^{\times}\left(r_{i/j}^{d}\right)^{\times}-\frac{1}{2}\left(\Theta_{i/j}^{\times}\right)^2\left(r_{i/j}^{d}\right)^{\times} & -\Theta_{i/j}^{\times}+\frac{1}{2}\left(\Theta_{i/j}^{\times}\right)^2 \end{bmatrix}+ \\ & +O(3) \end{aligned} \tag{A.11}$$

where $r^d_{i/j}$ is constant, Θ and p are the rotation and translation parts of the exponential coordinate vector X, and the Taylor expansions for $\sin\theta/\theta$ and $(1-\cos\theta)/\theta^2$ are employed to retrieve the results.